DE-FG05-80ET-53088-684 IFSR #684

Magnetic Viscosity by Localized Shear Flow Instability in Magnetized Accretion Disks

R. MATSUMOTO
Department of Physics, Faculty of Science
Chiba University
1-33 Yaoi-cho,
Inage-ku, Chiba 263, Japan
and
T. TAJIMA
Institute for Fusion Studies
The University of Texas at Austin
Austin, Texas 78712

January 1995

MAGNETIC VISCOSITY BY LOCALIZED SHEAR FLOW INSTABILITY IN MAGNETIZED ACCRETION DISKS

R. Matsumoto* and T. Tajima

Institute for Fusion Studies, The University of Texas at Austin

Austin, Texas 78712

(Received Aug. 18, 1993 ; accepted Dec., 1994)

January 9, 1995

Abstract

Differentially rotating disks are subject to the axisymmetric instability for perfectly conducting plasma in the presence of poloidal magnetic fields (Balbus & Hawley 1991). For nonaxisymmetric perturbations, we find localized unstable eigenmodes whose eigenfunction is confined between two Alfvén singularities at $\omega_d = \pm\omega_A$, where ω_d is the Doppler-shifted wave frequency, and $\omega_A = k_\parallel v_A$ is the Alfvén frequency. The radial width of the unstable eigenfunction is $\Delta x \sim \omega_A/(Ak_y)$, where A is the Oort's constant, and k_y is the azimuthal wave number. The growth rate of the fundamental mode is larger for smaller value of k_y/k_z. The maximum growth rate when $k_y/k_z \sim 0.1$ is $\sim 0.2\Omega$ for the Keplerian disk with local angular velocity Ω. It is found that the purely growing mode disappears when $k_y/k_z > 0.12$. In a perfectly conducting disk, the instability grows even when the seed magnetic field is infinitesimal. Inclusion of the resistivity, however, leads to the appearance of an instability threshold. When the resistivity η depends on the instability-induced turbulent magnetic fields $\delta\mathbf{B}$ as $\eta(\langle\delta B^2\rangle)$, the marginal stability condition self-consistently determines the α parameter of the angular momentum transport due to the magnetic stress. For fully ionized disks, the

*On leave from Department of Physics, Faculty of Science, Chiba University, 1-33 Yayoi-cho, Inage-ku, Chiba 263, Japan

magnetic viscosity parameter α_B is between 0.001 and 1. Our three-dimensional MHD simulation confirms these unstable eigenmodes. It also shows that the α parameter observed in simulation is between 0.01 and 1, in agreement with theory. The observationally required smaller α in the quiescent phase of accretion disks in dwarf novae may be explained by the decreased ionization due to the temperature drop.

Subject headings: accretion, accretion disks — hydromagnetics — instabilities — plasmas

1 INTRODUCTION

In conventional accretion disk models (e.g., Shakura & Sunyaev 1973), the α prescription of the viscosity is adopted. In this prescription the component of the stress-energy tensor $\tau_{\varpi\varphi}$ is equated to αP, where P is the pressure, which may include the radiation pressure. The $\tau_{\varpi\varphi}$ component contributes to the radial angular momentum transport. Thus the viscosity parameter α determines the time scale of the evolution of accretion disks.

In dwarf novae, by fitting the theoretical and observed durations of the quiescent phase and the bursting phase, it is suggested that α is of the order of 0.1 during the bursting phase; that on the other hand, α is about 0.02 in the quiescent phase (Cannizzo, Shafer, & Wheeler 1988). Since the molecular viscosity cannot provide such a high rate of angular momentum transport, various models of anomalous viscosity have been pushed forward; the convective turbulence (Lin & Papaloizou 1980; Kley, Papaloizou & Lin 1993), the global hydrodynamic shear flow instability (e.g., Papaloizou & Pringle 1984; Drury 1985; Goldreich, Goodman, & Narayan 1986; Kato 1987; Glatzel 1987), and the hydromagnetic turbulence (e.g., Eardley & Lightman 1975; Ichimaru 1977; Pudritz 1981; Kato 1984; Kato & Horiuchi 1985, 1986). Although the hydrodynamic shear flow instability has been studied extensively as a possible mechanism of generating turbulence in accretion disks, its contribution to α was shown to be only $O(10^{-3})$ in geometrically thin Keplerian disks (Kaisig 1989). Another model of angular momentum transport is the magnetic braking due to the emission of torsional Alfvén waves along large-scale poloidal magnetic fields in star forming regions or in active galactic nuclei (Mouschovias & Paleologou 1981; Uchida & Shibata 1985; Shibata & Uchida 1986; Uchida *et al.* 1991; Stone & Norman 1994). In this paper, we will concentrate on the angular momentum transport inside the disk and will not consider the exchange of angular momentum between the disk and external medium.

In hydromagnetic models of turbulent viscosity, the angular momentum is transported inside the disk by the magnetic stress incurred by fluctuating magnetic fields. Balbus & Hawley (1991) pointed out the importance of the local magnetic shearing instability on the generation of fluctuating magnetic fields. When a differentially rotating gas cylinder is threaded by sufficiently weak poloidal magnetic fields, it becomes unstable against axisymmetric perturbations, undulating the magnetic field lines (Velinhov 1959; Chandrasekhar 1961). When the disk is perfectly conducting, the maximum growth rate of this instability is of the order of the angular velocity of the disk Ω, even if the strength of the magnetic field approaches 0 (Balbus & Hawley 1991). Although the local stability analysis by Balbus & Hawley (1991) was questioned by Knobloch (1992), the normal mode analysis by Kumar *et al.* (1994) showed that unstable axisymmetric eigenmodes exist. Nonlinear ideal MHD simulations (Hawley & Balbus 1991, 1992; Hawley, Gammie, & Balbus 1994) also confirmed the presence of this robust instability. In the local incompressible limit, Goodman & Xu (1994) found an exact solution of the axisymmetric magnetic shearing instability that grows exponentially in the nonlinear stage. The resulting predominantly toroidal magnetic field can also be subject to nonaxisymmetric magnetic shearing instabilities (Balbus & Hawley 1992; Vishniac & Diamond 1992; Hawley *et al.* 1994) and other parasitic instabilities (Goodman & Xu 1994). By adopting the shearing coordinates (Goldreich & Lynden-Bell 1965) which has conventionally been used to study the amplification of global nonaxisymmetric waves in differentially rotating disks, Balbus & Hawley (1992) numerically showed that perturbations can grow significantly even when unperturbed magnetic fields are purely toroidal. Hawley *et al.* (1994) showed by three-dimensional MHD simulations that the two channel flow (Hawley & Balbus 1992; Goodman & Xu 1994) created by the axisymmetric magnetic shearing instability breaks up by nonaxisymmetric effects.

In Sec. 2, we develop the theoretical framework for modes in the presence of shear flows. We show that nonaxisymmetric unstable eigenmodes exist in differentially rotating mag-

netized disks. The origin of these eigenmodes is the trapping of Alfvén waves between two Alfvén singularities where the Doppler shifted wave frequency equals to the Alfvén frequency. These modes we find are distinct from those by Balbus & Hawley (1992), which were global noneigenmodes. Our linear theory finds that the instability now has the threshold with respect to the magnetic field strength in the presence of a small but finite resistivity. On the other hand the presence of finite viscosity does not change the qualitative behavior of the instability. The growth of turbulent magnetic fields due to this instability and its effect on anomalous resistivity are pronounced and discussed in Sec. 3. Even when the original resistivity is small enough to allow the instability, the enhanced resistivity by the instability-induced magnetic fields can lead to the stabilization of the instability. The strength of the fluctuating magnetic fields and the resulting magnetic stress are determined by applying the marginal stability theory (e.g., Manheimer & Boris 1977). In Sec. 4 we carry out three-dimensional MHD simulations of magnetic shear flow instabilities. These results on unstable parameter regimes, growth rates, eigenmodes etc. are in a good agreement with our linear theory of Sec. 2. The nonlinear evolutions observed in Sec. 4 such as the turbulent state, saturation level, the magnetic viscosity etc. are in a reasonable agreement with our nonlinear theory of Sec. 3. The astrophysical implications are discussed in Sec. 5.

2 LINEAR STABILITY ANALYSIS

2.1 Basic Equations

Since the compressibility is not important for magnetic shearing instability (Balbus & Hawley 1991), we assume an incompressible fluid for simplicity. The basic MHD equations in the frame rotating with angular velocity $\mathbf{\Omega}$ are

$$\frac{\partial \mathbf{v}}{\partial t} + (\mathbf{v}\cdot\nabla)\mathbf{v} = -\frac{1}{\rho}\nabla P + \frac{(\nabla\times\mathbf{B})\times\mathbf{B}}{4\pi\rho} + \mathbf{g} + 2\mathbf{v}\times\mathbf{\Omega} + (\mathbf{\Omega}\times\mathbf{r})\times\mathbf{\Omega} + \nu\nabla^2\mathbf{v}, \quad (1)$$

$$\frac{\partial \mathbf{B}}{\partial t} = \nabla \times (\mathbf{v} \times \mathbf{B}) + \eta \nabla^2 \mathbf{B}, \tag{2}$$

and

$$\nabla \cdot \mathbf{v} = 0, \tag{3}$$

where ν is the kinematic viscosity, η the electric resistivity, $\mathbf{g}$ the gravitational acceleration, and $\mathbf{r}$ the position vector. Other symbols have their usual meanings. We assumed that η are ν are spatially uniform.

We use the local Cartesian coordinate (x, y, z) in the rotating frame where x-axis is in the radial direction, the y-axis in the azimuthal direction, and the z-axis is parallel to $\mathbf{\Omega}$. The uniform velocity shear $v_y = -2Ax$ is assumed, where A is the shear rate, which equals to $3\Omega/4$ in a Keplerian disk. We neglect the gravity in the z-direction.

Theoretical approaches to the mode growth in a system with a velocity shear depend on the ratio of the shear scale-length L_s and the relevant wavelength L_n. For the global spiral pattern in galaxies whose wavelength is much longer than the shear scale length ($s = L_n/L_s \gg 1$), the WKB method is not appropriate. Goldreich & Lynden-Bell (1965) studied the growth of the spiral mode in self-gravitating gas disks by assuming the dependence $\widetilde{\phi}(x,t) = \widehat{\phi}(t) \exp[i(k_x(t)x + k_y y)]$, where $k_x(t) = k_x(0) + 2Ak_y t$. Since $\widetilde{\phi}(x,t)$ only depends on t along the line $y = -k_x(t)x/k_y$, the perturbation describes a long-wavelength mode along the direction swinging from the leading side ($t = -\infty$) to the trailing side ($t = \infty$) with the fluid. The amplification factor of perturbations imposed at $t = -\infty$ can be obtained by time-integrating the linearized equations. Balbus & Hawley (1992) followed this technique to study the growth of nonaxisymmetric perturbations in magnetized accretion disks. They showed that the growth of the swinging perturbation can occur not only for disks with poloidal seed magnetic fields but for disks with purely toroidal seed magnetic fields. Similar technique has been applied by Miller *et al.* (1994) to the velocity shear stabilization of the toroidally coupled ballooning mode which limits the plasma β in tokamaks, and by Fogglizzo

& Tagger (1994) to the velocity shear stabilization of the Parker instability, a sister mode of the ballooning instability. Note that for these modes, too, $s = L_n/L_s \gg 1$. Since the eikonal is time dependent, the solutions by Goldreich & Lynden-Bell (1965) are not eigenmode solutions. The temporally growing modes in this category are often said to be convectively unstable. They do not, however, have eigenmodes.

When $s = L_n/L_s \ll 1$, the WKB method may be used to determine the response to a localized fixed-frequency excitation of a shearing plasma (e.g., Tajima *et al.* 1991; Waelbroeck *et al.* 1994). It should be emphasized that unstable eigenmodes can exist even if the velocity shear is significant. One such example is the drift acoustic wave instabilities in the presence of sheared flows where exact eigenfunctions have been obtained (Waelbroeck *et al.* 1992). Another example is the nonaxisymmetric hydrodynamical shear flow instability in accretion disks (e.g., Papaloizou & Pringle 1984; Drury 1985). In nonmagnetized, nonself-gravitating differentially rotating disks, spontaneous growth of nonaxisymmetric modes occurs by the overreflection of waves at the corotation resonance where $\omega/k_y = v_y$ (Drury 1985; Goldreich, Goodman, & Narayan 1986; Kato 1987). When the disk has a reflecting edge on the same side where overreflection occurs, the disk becomes unstable. By imposing the appropriate boundary conditions, several authors have obtained standing, growing modes as solutions of the eigenvalue problem (e.g., Goldreich, Goodman, & Narayan 1986; Kato 1987; Hanawa 1987; Glatzel 1987). When unstable eigenmodes exist, they will eventually dominate over transiently amplified waves.

In this paper, however, we are interested in localized instabilities and their subsequent turbulence that are not influenced by the disk edge boundaries. These determine the local property of plasma transport such as the angular momentum transport, i.e, the problem of the viscosity of differentially rotating disks. Thus we adopt the eigenmode analysis formulation suitable for localized instabilities. Note that in the presence of shear flow localized modes show strong wave absorption characteristics and deviate sharply from sinusoidal be-

haviors and that thus a simpler and more naive local Fourier analysis is not adequate or at least only approximate. On the other hand, such problems as the global pattern of spiral arm magnetic fields need the temporal domain formulation mentioned earlier and are not in the scope of the present paper.

2.2 Formal Solutions of the Initial-value and the Eigenvalue Problem

The stability of rotating disks can be studied by linearizing the basic equations around the equilibrium state and looking for solutions of the form $\tilde{\phi}(x,t)\exp[i(k_y y + k_z z)]$. The Laplace transform of the perturbation, $\overline{\phi}(x,\omega)$, is employed

$$\overline{\phi}(x,\omega) = \int_0^\infty dt\tilde{\phi}e^{i\omega t} \tag{4}$$

for $\mathrm{Im}(\omega) > 0$. Let the basic equation take the form

$$\frac{d^2\overline{\phi}}{dx^2} + L(x,\omega)\overline{\phi} = \Gamma(x,\omega). \tag{5}$$

The initial condition enters through the function $\Gamma(x,\omega)$. This equation may be solved in terms of Greene's function,

$$G(x,\hat{x},\omega) = [\overline{\phi}_+(x,\omega)\overline{\phi}_-(\hat{x},\omega)H(x-\hat{x}) + \overline{\phi}_+(\hat{x},\omega)\overline{\phi}_-(x,\omega)H(\hat{x}-x)]/D(\omega). \tag{6}$$

Here $\overline{\phi}_+$ and $\overline{\phi}_-$ are the solutions of the homogeneous equation vanishing at $+\infty$ and $-\infty$ respectively, and $H(x)$ is the Heaviside step function. These $\overline{\phi}_+$ and $\overline{\phi}_-$ are the standard eigenfunctions in the standard eigenmode analysis (Waelbroeck *et al.* 1994). $D(\omega)$ is the Wronskian of these solutions, $D(\omega) = \overline{\phi}'_+(x,\omega)\overline{\phi}_-(x,\omega) - \overline{\phi}_+(x,\omega)\overline{\phi}'_-(x,\omega)$. Having introduced Greene's function in Eq. (6), we can show that this analysis can be useful even for the cases where no eigenmode exists. The solution is

$$\overline{\phi}(x,\omega) = \int_{-\infty}^{\infty} d\hat{x}G(x,\hat{x},\omega)\Gamma(\hat{x},\omega),$$

and the response as a function of time t is then

$$\widehat{\phi}(x,t) = \frac{1}{2\pi}\int_{-\infty+ic}^{\infty+ic} d\omega e^{-i\omega t}\overline{\phi}(x,\omega), \tag{7}$$

where the Laplace inversion integral extends over the contour lying above all the singularities in the integrand. Equation (7) can have temporally growing solutions even if there is no eigenvalue and eigenfunction to Eq. (5). In fact the global spiral modes of Goldreich & Lynden-Bell are such a case. Still this formal solution of the initial value problem through $\overline{\phi}_+$ and $\overline{\phi}_-$ is equivalent to the temporal formulation by Goldreich & Lynden-Bell (1965) if we assume the functional form $\widetilde{\phi}(x,t) = \widehat{\phi}(t)\exp[i(k_x(0) + 2Ak_y t)x]$.

Unstable eigenmodes occur when the Wronskian has a zero in the upper complex ω plane. It means that the solution vanishing as $\xi \to -\infty$ is proportional to that vanishing as $\xi \to \infty$, or that there exists a globally well-behaved solution. The latter constitutes the standard eigenmode problem. In the below we consider the localized eigenmode problem, as discussed here and will find exponentially growing localized eigenfunctions. Such modes are distinct from the temporal domain modes discussed by Balbus & Hawley (1992). On the other hand Balbus & Hawley (1991) treated no radial eigenfunction structures.

2.3 Eigenmode Solutions of the Wave Equation

In this subsection we derive the wave equation in differentially rotating magnetized disks and solve the eigenvalue problem. In the unperturbed state, the density, pressure, and magnetic fields are assumed to be uniform. By assuming that $v_x = v_z = 0$ in the unperturbed state, the unperturbed momentum equation is

$$\mathbf{g} + 2\mathbf{v}_0 \times \mathbf{\Omega} + (\mathbf{\Omega} \times \mathbf{r}) \times \mathbf{\Omega} = 0. \tag{8}$$

We further assume that $B_x = 0$ in the unperturbed state. We linearize the basic equations and look for eigenmode solutions of the form $\widetilde{\phi}(x,t)\exp[i(k_y y + k_z z)]$ according to the above

discussion. The Laplace transform of the momentum equation and the induction equation are

$$-i\omega_d\overline{\mathbf{v}} - 2A\overline{v}_x\widehat{y} - 2\overline{\mathbf{v}}\times\mathbf{\Omega} - \frac{(\mathbf{B}\nabla)\overline{\mathbf{b}}}{4\pi\rho} + \nabla\left(\frac{\mathbf{B}\overline{\mathbf{b}}}{4\pi\rho} + \frac{\delta\overline{p}}{\rho}\right) - \nu\nabla^2\overline{\mathbf{v}} = \widetilde{\mathbf{v}}(x,0), \tag{9}$$

and

$$-i\omega_d\overline{\mathbf{b}} + 2A\overline{b}_x\widehat{y} - (\mathbf{B}\nabla)\overline{\mathbf{v}} - \eta\nabla^2\overline{\mathbf{b}} = \widetilde{\mathbf{b}}(x,0), \tag{10}$$

where

$$\omega_d = \omega + 2Ak_y x \tag{11}$$

is the Doppler shifted frequency, $\overline{\mathbf{b}}$, $\overline{\mathbf{v}}$, and $\delta\overline{p}$ are Laplace transform of the magnetic field, velocity, and the pressure perturbations, respectively.

Substituting these results into the Laplace transform of the continuity equation $\nabla\cdot\mathbf{v} = 0$ yields the initial value equation

$$\omega_\eta^2\omega_{\eta\nu}^4\frac{d^2\overline{v}_x}{dx^2} + 4A\omega_A^2k_y\omega_\eta\omega_{\eta\nu}^2\frac{d\overline{v}_x}{dx} + \left[-(k_y^2+k_z^2)\omega_\eta^2\omega_{\eta\nu}^4 - 8A^2k_y^2\omega_A^2\omega_{\eta\nu}^2 + \kappa^2k_z^2\omega_\eta^2(\omega_\eta^2 + A\omega_A^2/\Omega_B)\right]\overline{v}_x = \Gamma(x,\omega) \tag{12}$$

where

$$\omega_\eta = \omega_d + i\eta(k_y^2 + k_z^2 - \frac{d^2}{dx^2}), \tag{13}$$

$$\omega_\nu = \omega_d + i\nu(k_y^2 + k_z^2 - \frac{d^2}{dx^2}), \tag{14}$$

and

$$\omega_{\eta\nu}^2 = \omega_\eta\omega_\nu - \omega_A^2. \tag{15}$$

Here $\Omega_B = \Omega - A$, $\kappa = 2(\Omega\Omega_B)^{1/2}$ is the epicyclic frequency, and ω_A is the Alfvén frequency

$$\omega_A^2 = \frac{(\mathbf{k}\cdot\mathbf{B})^2}{4\pi\rho} = k_\parallel^2 v_A^2. \tag{16}$$

The initial condition enters through the right-hand side of Eq. (12).

First, we consider the case when there is no dissipation ($\eta = \nu = 0$). The homogeneous part of Eq. (12) reduces to the second order differential equation as

$$\frac{d^2\bar{v}_x}{dx^2} + \frac{4A\omega_A^2 k_y}{\omega_d(\omega_d^2 - \omega_A^2)}\frac{d\bar{v}_x}{dx} + \left[-(k_y^2 + k_z^2) - \frac{8A^2k_y^2\omega_A^2}{\omega_d^2(\omega_d^2 - \omega_A^2)} + \kappa^2 k_z^2 \frac{\omega_d^2 + A\omega_A^2/\Omega_B}{(\omega_d^2 - \omega_A^2)^2}\right]\bar{v}_x = 0. \quad (17)$$

It is noted that in the presence of shear flows the eigenmode equation such as Eq. (17) does not take the self-adjoint form anymore. Thus the eigenvalues ω are not guaranteed to be real or pure imaginary. We express Eq. (17) in terms of

$$\xi = \frac{2Ak_y x}{\omega_A} \quad (18)$$

as

$$\frac{d^2\bar{v}_x}{d\xi^2} + \frac{2\omega_A^3}{\omega_d(\omega_d^2 - \omega_A^2)}\frac{d\bar{v}_x}{d\xi} + \left[-\left(1 + \frac{1}{q}\right)\left(\frac{\omega_A}{2A}\right)^2 - \frac{2\omega_A^4}{\omega_d^2(\omega_d^2 - \omega_A^2)} + \left(\frac{\kappa}{2A}\right)^2\left(\frac{\omega_A^2}{q}\right)\frac{\omega_d^2 + A\omega_A^2/\Omega_B}{(\omega_d^2 - \omega_A^2)^2}\right]\bar{v}_x = 0 \quad (19)$$

where

$$q = \frac{k_y^2}{k_z^2}. \quad (20)$$

This differential Eq. (19) has two singularities at $\omega_d = \pm\omega_A$. These are the shear Alfvén singularities where the absorption and mode conversion of Alfvén waves take place (e.g., Ross *et al.* 1982). The locations of Alfvén singularities in the complex plane are

$$\xi_A = \pm 1 - \frac{\omega}{\omega_A}. \quad (21)$$

By applying the Frobenius method around $\omega_d = \pm\omega_A$ (or $\xi = \xi_A$), and solving the indicial equation, we find that the exponent s in the series expansion

$$\bar{v}_x(\xi) = \sum_{n=0}^{\infty} a_n(\xi - \xi_A)^{n+s}$$

becomes complex. Thus the solutions which pass through these points are singular (called regular singular points). The corotation point $\omega_d = 0$ (or $\xi_c = -\omega/\omega_A$) appears to be also

singular in Eq. (19). However, by solving the indicial equation, we find that the solution is regular at the corotation point.

The solutions of Eq. (19) which vanish as $\xi \to \pm\infty$ have an asymptotic form

$$\overline{v}_x \propto \exp[\mp(1+1/q)^{1/2}\omega_A \xi/(2A)]. \tag{22}$$

We now numerically look for eigenmodes whose eigenfunction connects these asymptotic solutions. At the numerical boundaries at $\xi = \pm 5$, we impose a boundary condition $\overline{v}_x'/\overline{v}_x = k_\mp$, where $k_\mp$ are negative and positive solutions of the quadratic equation given by inserting the functional form $\overline{v}_x \propto \exp(k_\pm x)$ into Eq. (19). The eigenvalues and eigenfunctions which satisfy these boundary conditions are obtained through the shooting method.

Figure 1 shows examples of eigenfunctions $\overline{v}_x$ for the Keplerian disk ($A/\Omega = 3/4$) when $\omega_A = 0.1\Omega$ and $q = 0.01$. The solid curve and the dashed curve represent the real part and the imaginary part of the eigenfunction, respectively. Figure 1a is for the fundamental mode, and Figure 1b is for the next nodal mode. Since the eigenvalues are pure imaginary ($\omega = 0.069\Omega i$ for the fundamental mode, and $\omega = 0.036\Omega i$ for the next nodal mode) in these cases, the eigenfunctions are symmetric (or antisymmetric) with respect to $\xi = 0$. The eigenfunctions are confined between two Alfvén singularities located at $\xi = \pm 1$ where the Alfvén waves vanish. The standing growing mode appears between these singularities. The distance between these resonance points is $\Delta x \sim \omega_A/(Ak_y)$. When the unperturbed field is purely toroidal, we find $\Delta x \sim v_A/A \sim (v_A/C_s)(\Omega/A)H$, where H is the thickness of the disk and C_s is the sound speed. Thus when $v_A \ll C_s$, the mode is localized in the radial direction with the mode width small compared to the disk thickness. When the unperturbed magnetic fields have poloidal components, Δx is proportional to $k_\parallel/k_y$. In such a case, the standing wave can have a large radial extent for nearly axisymmetric perturbations ($k_y \ll k_\parallel$). The purely toroidal field is a special case in which Δx is independent of $q = k_y^2/k_z^2$.

Figure 2 shows the dependence of eigenvalue in the Keplerian disk on ω_A and q. When

purely growing mode exists, we find two unstable branches, which correspond to the fundamental mode (the upper branch in figure 2) and its next nodal mode (the lower branch in figure 2). These two branches merge at $\omega_A = \omega_m$ and form complex eigenvalues with $\mathrm{Re}(\omega) \neq 0$. Recall that the differential equation with shear flows is not self-adjoint. The dashed curves show the real part of the eigenvalues. The maximum growth occurs when $\omega_A \sim \Omega$. When $q = 0.01$, the maximum growth rate of the fundamental mode is $\sim 0.2\Omega$. This value is less than a half the maximum growth rate of the axisymmetric magnetic shearing instability. The reduction of the maximum growth rate for nonaxisymmetric perturbations is interpreted to arise from the radial confinement of the mode. The growth rate of the modes decreases with increasing q. We find that the purely growing mode disappears when $q > 0.015$. Although unstable modes with complex eigenvalues still survive, their significance will be less than the purely growing mode partly because their growth rate is lower. Thus we expect that unstable eigenmodes whose azimuthal wavelength is much longer than the vertical wavelength will become dominant.

In the regime where $\omega_A \ll \Omega$, the growth rate of the fundamental mode is roughly proportional to ω_A and we write the growth rate as

$$\gamma^2 = f(q)\omega_A^2. \tag{23}$$

The proportionality coefficient $f(q)$ is a decreasing function of q and $f(q) \sim 0.5$ when $q \sim 0.01$. With dissipation, corresponding expressions with η and ν can be derived.

2.4 Local Dispersion Relation

Here we compare the shooting code results in Sec. 2.3 with the local (Fourier) dispersion relation. By replacing d/dx in Eq. (12) with ik_x in a region around $x = 0$, the local dispersion relation is reduced to

$$\omega_\eta^2(\omega_\eta\omega_\nu - \omega_A^2)^2 - \omega_I^2\omega_\eta^2(\omega_\eta^2 + A\omega_A^2/\Omega_B) + (8A^2q_y - 4Aq_{xy}i\omega_\eta)\omega_A^2(\omega_\eta\omega_\nu - \omega_A^2) = 0, \tag{24}$$

where $\omega_I^2 = \kappa^2 k_z^2/k^2, k^2 = k_x^2 + k_y^2 + k_z^2$, $q_y = k_y^2/k^2$, and $q_{xy} = k_x k_y/k^2$. For axisymmetric perturbations ($k_y = 0$) in a nondissipative disk ($\eta = \nu = 0$), Eq. (24) reproduces the local dispersion relation derived by Balbus & Hawley (1991). In such a perturbation, unstable modes appear when $\omega_A^2 < (A/\Omega_B)\omega_I^2$.

When the unperturbed magnetic field is toroidal ($B_x = B_z = 0$), the approximate solutions of Eq. (24) in the regime $|\gamma| \sim \omega_A \ll \omega_I$ yields the growth rate for a disk with $\eta = \nu = 0$ as

$$\gamma^2 = \frac{A}{2\Omega_B}\left[1 - \frac{2A}{\Omega}q \pm \sqrt{1 - 4\left(1 + \frac{\Omega_B}{\Omega}\right)q + \left(\frac{2A}{\Omega}\right)^2 q^2}\right]\omega_A^2. \tag{25}$$

In the Keplerian disk, purely growing modes appear only when $q < 2/9$. This result is qualitatively consistent with the numerical results of the eigenmode analysis discussed in Sec. 2.3.

2.5 Threshold of the Instability

First, we consider a case where the unperturbed magnetic fields are purely poloidal ($B_x = B_y = 0$). The criterion for the instability for axisymmetric ($k_y = 0$) perturbations is

$$(\omega_A^2 + \eta\nu k^4)^2 + \omega_I^2(\eta^2 k^4 - \frac{A}{\Omega_B}\omega_A^2) < 0. \tag{26}$$

When $\eta = 0$, we have seen that unstable modes appear for weak magnetic fields which satisfy $B_z^2 < 4\pi\rho(A/\Omega_B)(\kappa^2/k^2)$. There is no instability threshold for B_z from below, as $B_z = 0+$ satisfies this condition (Balbus & Hawley 1991). Note, however, that when $B_z = 0$ there is no instability.

When $\eta \neq 0$, however, there is a critical value for B_z

$$B_{zc}^2 = 4\pi\rho\left(\frac{\Omega_B}{A}\right)\frac{\eta^2 k^4}{k_z^2}, \tag{27}$$

below which the second term in the left hand side of Eq. (26) is positive. We now find that the Balbus-Hawley mode is stabilized for sufficiently weak seed magnetic fields or sufficiently

large resistivity. Such a threshold does not appear when $\eta = 0$ even if $\nu \neq 0$, and thus we conclude that the kinematic viscosity does not play an essential role for the stabilization of the Balbus-Hawley mode, but the resistivity does.

Next, we consider the toroidal field case. Approximate growth rates may be obtained by solving the local dispersion relation (Eq. (24)). Figure 3 shows the growth rate when $k_x H = 2\pi(A/\Omega)(C_s/v_A)$, $k_z H = \pi$, $q = 0.01, 0.025$ and $\nu = 0$. Here k_x is equated to the width of the unstable eigenfunction. Thin curve and thick curve show the growth rates of the purely growing mode for $\eta = 0$ and $\eta = 10^{-4} C_s H$, respectively. Comparing the growth rates for $\eta = 0$ with the eigenvalues in figure 2, we find that the local dispersion relation gives reasonable estimates of the eigenvalues. The coincidence with the shooting code result occurs because the purely growing modes are localized between two Alfvén singularities (see figure 1).

When $\eta \neq 0$, unstable modes disappear when ω_A is below a threshold. The threshold for the upper branch is $\omega_A \sim 0.05\Omega$ when $q = 0.01$. This threshold is close to that determined by equating the nonresistive growth rate ($\gamma \sim k_y v_A$) with the resistive damping rate (ηk^2).

3 MAGNETIC FLUCTUATIONS AND VISCOSITY IN ACCRETION DISKS

When charged particles, electrons in particular, move in stochastic magnetic fields, their orbits (or streamlines) in such fields become diffusive. This diffusiveness may arise both from the field aligned directional motion and from that perpendicular to the field. Such diffusive orbits may give rise to effective scattering of electrons and thus to effective resistivity. In general such fluctuating magnetic field effects can be incorporated by a quasilinear theory. Thus the resistivity becomes a function of fluctuations $\langle \delta B^2 \rangle$ as $\eta = \eta(\langle \delta B^2 \rangle)$ in a generic expression. As concrete examples of such an expression, we employ one by Ichimaru (1975) and one by Horton, Tajima & Galvao (1984) in the following. Although details of their

theories and thus their formalisms are different, a common nonlinear feature exists, as both theories have the quadratically nonlinear δB dependence of η.

Although the collisional resistivity η_0 of the disk is small to allow the instability, the enhanced (anomalous) resistivity η due to magnetic fluctuations becomes large enough to saturate the instability when the turbulence sets in. Thus, the strength of magnetic fluctuations is determined near or at the marginal stability dictated by this anomalous resistivity when the unstable hydromagnetic modes are robust. The concept of the marginal stability has been invoked to fusion plasma problems (e.g., Manheimer & Boris 1977; Tajima *et al.* 1994) and magnetic diffusion problems during the star formation (Norman & Heyvaerts 1985). When the governing instability is (magneto)hydrodynamic and encompasses many mode surfaces, the system can reach a quasisteady state by making it close to but slightly above the marginal stability (To be precise, the small deviation away from the marginal is determined by the input rate of energy to the disk such as the binary star mass injection etc.). Otherwise, large scale "vortices" exerting strong modulating influence on the background shear profile can be quickly transported away (intermittent burst and returns to a quasi-steady state). In this way the level of magnetic fluctuations is self-consistently determined once the global conditions of the disk are given.

3.1 Anomalous Resistivity Model 1

First, we adopt the resistivity expression by Ichimaru (1975),

$$\eta = \frac{c^2}{4\pi\sigma} = \left(\frac{\pi}{2}\right)^{1/2} \frac{1}{4\pi n_e m C_s} \sum_k \int d\omega \frac{k_J^2}{k^3} \left\langle |b^2|(\mathbf{k},\omega) \right\rangle, \tag{28}$$

where σ is the electrical conductivity, m the mass of ions, n_e the number density of electrons, $\langle |b^2|(\mathbf{k},\omega)\rangle$ is the spectral intensity of the magnetic fluctuations, and k_J is the component of wave vector parallel to the mean electric current. This expression has been used to model the magnetic turbulence in accretion disks by Ichimaru (1977) and Kato (1984). The

three-dimensional computation of Hawley *et al.* (1994) and ours in Sec. 4 indicate numerous x-point like structures in the nonlinear stage of the magnetic shearing instability. When the plasma is fully ionized ($n = n_e$), we set $\rho = n_e m$. As we have shown in Sec. 2.3, the magnetic fluctuations generated by the magnetic shearing instability are highly anisotropic such that $k_y^2 \ll k_z^2 \sim k_x^2$. The mean electric current is predominantly in the x-z plane because we find the toroidal component of magnetic fields dominate over the poloidal component once the instability sets in.

By assuming that the magnetic fluctuations have a spectrum peaked around $\mathbf{k}_{\max}$, and by denoting

$$\left\langle \delta B^2 \right\rangle = \int d\omega \left\langle |b^2|(\mathbf{k}_{\max}, \omega) \right\rangle , \tag{29}$$

we obtain

$$\eta = \left(\frac{\pi}{2}\right)^{1/2} \frac{1}{4\pi n_e m C_s} \left(\frac{k_J^2}{k^3}\right)_{\max} \left\langle \delta B^2 \right\rangle , \tag{30}$$

where $(k_J^2/k^3)_{\max}$ is evaluated at $\mathbf{k} = \mathbf{k}_{\max}$.

Since magnetic fields induced by the magnetic shearing instability eventually dominate over seed magnetic fields, we equate B^2 to $\langle \delta B^2 \rangle$ to evaluate the saturation level. The saturation level of magnetic fluctuations can be determined by equating the growth rate γ of the instability with the anomalous resistivity damping ηk^2. By using Eq. (23) for γ and Eq. (30) for η, we obtain

$$\frac{\langle \delta B^2 \rangle}{4\pi n_e m C_s^2} = \chi_e \left(\frac{2}{\pi}\right) \left(\frac{k^2 k_z^2}{k_J^4}\right) \left(\frac{k_\parallel^2}{k_z^2}\right) f(q), \tag{31}$$

where $\chi_e = n_e/n$ is the ionization rate. The factor $k_\parallel^2/k_z^2$ is unity for purely poloidal field. For cases with a purely toroidal field $k_\parallel^2/k_z^2 = q$. In the marginally stable state $k_\parallel^2/k_z^2$ is between q and 1 because the magnetic fields are already perturbed.

As the disk plasma is close to the marginality, the magnetic viscosity parameter $\alpha_B = -\langle \delta B_x \delta B_y \rangle / (4\pi \rho C_s^2)$ may be approximately written by using the linearized momentum

equation (Eq. (9)) and linearized induction equation (Eq. (10)) with $\eta = \nu = 0$ as

$$\alpha_B = \chi_e \frac{\langle \delta B^2 \rangle}{4\pi n_e m C_s^2} \frac{-\left\langle \frac{\delta B_y}{\delta B_x} \right\rangle}{\left\langle \left(\frac{\delta B_y}{\delta B_x} \right)^2 \right\rangle + \left\langle \left(\frac{\delta B_z}{\delta B_x} \right)^2 \right\rangle + 1}, \tag{32}$$

where

$$\left\langle \frac{\delta B_y}{\delta B_x} \right\rangle = \frac{-2\Omega\gamma + (\gamma^2 + \omega_A^2 - 4A\Omega)(k_y/k_x)}{\gamma^2 + \omega_A^2 + 2\Omega\gamma(k_y/k_x)}, \tag{33}$$

and

$$\left\langle \frac{\delta B_z}{\delta B_x} \right\rangle = -q^{1/2} \frac{(\gamma^2 + \omega_A^2)(k_x/k_y + k_y/k_x + 2A/\gamma)}{\gamma^2 + \omega_A^2 + 2\Omega\gamma(k_y/k_x)}. \tag{34}$$

When deriving these equations, we replaced d/dx by ik_x. This local approximation is accurate to the extent we showed in Sec. 2.5. The notations $\langle \delta B_x \delta B_y \rangle$ etc. denote the spatial average.

The instability-induced velocity fields also contribute to the radial angular momentum transport. The viscosity parameter corresponding to the Reynolds stress $\rho \langle v_x v_y \rangle$ due to this instability is expressed as

$$\alpha_v = \frac{\langle v_x v_y \rangle}{C_s^2} = -\alpha_B \left(\frac{\gamma^2}{\omega_A^2} \right) \frac{\langle v_y / v_x \rangle}{\langle \delta B_y / \delta B_x \rangle}, \tag{35}$$

where

$$\left\langle \frac{v_y}{v_x} \right\rangle = \left\langle \frac{\delta B_y}{\delta B_x} \right\rangle + \frac{2A}{\gamma}. \tag{36}$$

Since $k_y \ll k_x$, we can evaluate as

$$\left\langle \frac{\delta B_y}{\delta B_x} \right\rangle \sim \frac{-2\Omega\gamma}{\gamma^2 + \omega_A^2} \sim \frac{-2f(q)^{1/2}}{f(q) + 1} \left(\frac{\Omega}{\omega_A} \right),$$

and

$$\left\langle \frac{\delta B_z}{\delta B_x} \right\rangle \sim -\frac{k_x}{k_z}.$$

When $f(q) \sim 1$, $k_x \sim k_z$, $\omega_A \sim \Omega$, and $\chi_e = 1$, the magnetic viscosity α_B is a third of the magnetic fluctuation $\langle \delta B^2 \rangle / (4\pi n_e m C_s^2)$, and $\alpha_v \sim (2A/\Omega - 1)\alpha_B$.

In Table 1, we show the dependence of α_B and α_v on the shear parameter A based on this Model 1. When the poloidal field is dominant ($k_\parallel^2/k_z^2 \sim 1$), the magnetic fluctuation (Eq. (31)) is maximized when $q = 0$. The functional value $f(q)$ is approximately given by Eq. (24) as $f(q=0) = A/(\Omega - A)$. The magnetic fluctuation level is determined by assuming that $k_J^2 \sim k_z^2 \sim k^2$ and $\chi_e = 1$. The maximum growth rate $\gamma = A$ and the corresponding ω_A $[\omega_A^2 = A(\Omega + \Omega_B)]$ are substituted into Eqs. (33), (34), and (36) to determine α_B and α_v. When the toroidal field is dominant ($k_\parallel^2/k_z^2 \sim q$), the magnetic fluctuation level is low when $q \ll 1$. By eigenmode analysis, we find that for a wide range of the shear parameter A, the function $qf(q)$ is maximized when $q = q_{\max} \sim 0.01$. We show $q_{\max}$ and $q_{\max} f(q_{\max})$ in the second and third column of Table 1(b). The magnetic fluctuation level for initially toroidal field case is determined by assuming $k_J^2 \sim k_x^2 \sim k_z^2 \sim k^2/2$ and $\chi_e = 1$. The maximum growth rate of the purely growing eigenmode and corresponding ω_A are used to determine α_B and α_v. The ratio of the wavenumbers k_y/k_x is determined from the width of unstable eigenfunction as $k_x \sim 2\pi A k_y/\omega_A$. When both the toroidal and the poloidal fields exist ($q < k_\parallel^2/k_z^2 < 1$), the magnetic viscosity will be between the values listed in Table 1(a) and Table 1(b).

3.2 Anomalous Resistivity Model 2

Next, we adopt the resistivity expression by Horton, Tajima, & Galvao (1984). They considered turbulent electron (and fluid) motions, which gave rise to electron diffusion as

$$\eta = \eta_0 + \Sigma_{k_\parallel} \frac{2k_| \langle \delta B^2 \rangle}{\gamma + \eta k^2}. \tag{37}$$

For the representative mode which contributes most to the right-hand side of Eq. (37), we obtain

$$\eta k^2 \sim \frac{\gamma}{2}\left[-1 + \sqrt{1 + \frac{8k_\parallel^2 \langle \delta B^2 \rangle k^2}{\gamma^2}}\right]. \tag{38}$$

When the growth rate γ is proportional to B according to Eq. (23), ηk^2 is proportional

to $\langle \delta B^2 \rangle^{1/2}$. By equating γ and ηk^2 the saturation level of magnetic fluctuations remains undetermined. This indicates that the magnetic fluctuations can grow up to $\omega_A \sim \Omega$ (if ω_A exceeds Ω, it is stable). The value of the viscosity parameter α_B will be then

$$\alpha_B = -\frac{\langle \delta B_x \delta B_y \rangle}{4\pi\rho C_s^2} < \frac{\langle \delta B^2 \rangle}{4\pi\rho C_s^2} \sim \frac{\omega_A^2}{k_\parallel^2 C_s^2} < \frac{1}{(k_\parallel H)^2}. \tag{39}$$

When the poloidal field is dominant, since $k_| H > \pi$, the magnetic viscosity is $\alpha_B \sim \mathrm{O}(0.1)$. When the toroidal field is dominant, $(k_| H)^2 = q(k_z H)^2 \sim n_z^2 \pi^2 q$ where n_z is the number of nodes in z-direction. Except for $n_z \leq 3$, the right-hand side of Eq. (39) is less than unity when $q \sim 0.01$. When only long wavelength modes in z-direction dominate the system ($n_z \leq 3$), other effects are likely to compete with what we consider here.

In a more complete treatment other independent variables (i.e., the pressure and thus the thickness of the disk and the flow shear) with the control parameters such as the energy input rate should be simultaneously solved along with $\langle \delta B^2 \rangle$ to determine the steady or (quasisteady) limiting cycle state. Such equations are generally similar to the prey-predictor system (Tout & Pringle 1992). Such relaxation oscillations (or bursts) might be related to observational high state — low state transitions and quasi-periodic luminosity variations believed to come from accretion disks around a neutron star or a black hole.

4 THREE DIMENSIONAL SIMULATION

We carried out fully nonlinear three-dimensional MHD simulation of accretion disks in the corotation frame of reference. The basic equations are the momentum Eq. (1) with $\nu = 0$, induction Eq. (2) and additionally the equation of continuity

$$\frac{\partial \rho}{\partial t} + \nabla(\rho \mathbf{v}) = 0, \tag{40}$$

equation of energy

$$\frac{\partial \rho\epsilon}{\partial t} + \nabla(\rho\epsilon \mathbf{v}) + p\nabla\mathbf{v} = \eta \mathbf{J}^2, \tag{41}$$

where $\mathbf{J}$ is the current density

$$\mathbf{J} = \frac{\nabla \times \mathbf{B}}{4\pi}, \tag{42}$$

and the equation of state

$$P = \rho\epsilon(\gamma_a - 1), \tag{43}$$

where γ_a is the adiabatic index. We use $\gamma_a = 5/3$ in this paper.

We adopt the shearing box model (Hawley *et al.* 1994) and impose the following boundary condition on the plane $x = 0$ and $x = L_x$ where L_x is the size of the simulation box in x-direction

$$f(x, y, z) = f(x + L_x, y - 2AL_x t, z). \tag{44}$$

This boundary condition was implemented by Wisdom & Tremaine (1988) to simulate the planetary rings, and later used by Hawley & Balbus (1992) and Hawley *et al.* (1994). The boundaries at $y = 0$, $y = L_y$, $z = 0$ and $z = L_z$ are periodic boundaries.

The initial condition is the same as the equilibrium model we adopted in Sec. 2. In the following, we use the units $C_s = \Omega = \rho_0 = 1$ where ρ_0 is the initial density. The unit of the length equals to the scale height H of the disk. To initiate the simulation, we imposed random perturbations for v_y and P at $t = 0$. The amplitudes of perturbations are $\delta v_y = 10^{-3} C_s$, and $\delta P = 10^{-3}\rho_0 C_s^2$.

The simulation code is based on the modified Lax-Wendroff method (Rubin & Burstein 1967) with artificial viscosity (Richtmyer & Morton 1967). The three-dimensional version of this code has been applied to the Parker instability in accretion disks (Matsumoto & Shibata 1992) and the emergence of magnetic flux in the solar atmosphere (Matsumoto *et al.* 1993, 1994). We dropped the artificial diffusion term from the induction equation and set $\eta = 0$ except the region where the current density is larger than a critical value $J_c = 100\rho_0^{1/2}\Omega$. The effective magnetic Reynolds number by numerical resistivity is the order of 10^5. The magnetic Reynolds number is artificially reduced to $O(10^2)$ in the current sheet where $|J| > J_c$.

In the following, we show the numerical results for a typical model (model T) starting with B_y alone with the Keplerian velocity shear ($A = 3/4\Omega$). The initial magnetic field is assumed to be uniform and purely toroidal. The initial plasma β ($= 8\pi P_0/B_0^2$) is 100. For these parameters, the radial extent of the most unstable eigenmode is theoretically expected to be $\Delta x = v_A/A \sim 0.2H$ (see Sec. 2). Thus we choose the size of the simulation box and the number of grid points such that we can numerically resolve the eigenmode. The size of the simulation box is $(L_x, L_y, L_z) = (0.5H, 2H, 0.5H)$. The number of grid points for this run is $(N_x, N_y, N_z) = (41, 41, 41)$.

Figure 4 shows isocontours of the azimuthal velocity perturbation $\delta v_y = v_y + 2Ax$ in the $z = 0.25H$ plane. After waves with very short radial wavelength appear ($t = 8.4/\Omega$), the mode whose radial wavelength is about $0.2H$ grows exponentially ($t = 11.2 - 16.4/\Omega$). The preferential growth of the perturbation with $\lambda_x = 0.2H$ is also seen in figure 5 in isocontours of δv_y in the x-z plane. The azimuthal wavelength of the exponentially growing mode is nearly the box size ($\lambda_y = 2H$), while the vertical wavelength is $\lambda_z \sim 0.3H$. These results are consistent with the linear stability analysis in Sec. 2. Figure 6 shows the time variation of B_x along the line $y = H$ and $z = 0.25H$. The growth of the mode around $x = -0.1H$ can be seen. Thus we conclude from both linear and nonlinear investigations that radially confined unstable eigenmode becomes dominant in the growth of the magnetic shearing instability in accretion disks. It should be noted that since we are using the shearing box periodic boundary condition, and allowable mode numbers do not restrict the mode rational surface (the center of the eigenmode x-position), there is no unique surface position x. Thus such eigenmodes excited at various x's will overlap each other. This is in fact seen in figure 4.

In the later stage ($t > 20/\Omega$), the growth of the eigenmode nearly saturates and the system shows more complex behavior. Figure 7 shows the magnetic field lines. Magnetic field lines are highly tangled up. This justified our physical picture of turbulent and chaotic magnetic field lines anticipated from linear theory in Sec. 2 and adopted for nonlinear theory

in Sec. 3. This feature was invoked to evaluate the saturation by enhanced resistivity.

Figure 8 shows the time history of $\alpha_B = -\langle B_x B_y \rangle / (4\pi P_0)$, $\alpha_v = \rho_0 \langle v_x v_y \rangle / P_0$, and $(\langle B^2 \rangle - B_0^2)/(8\pi P_0)$. These quantities increase exponentially during the growth of eigenmodes ($t = 8 - 20/\Omega$). Experimentally obtained growth rate in this stage is 0.23Ω. This growth rate is close to the maximum growth rate $\gamma_{\max} = 0.22\Omega$ for $q = 0.01$ obtained from eigenmode analysis (see figure 2). The magnetic viscosity α_B increases up to 0.020 while the kinematic viscosity α_v is about 0.005. These are within the range of the values we obtained in Sec. 3. We have also carried out simulation runs starting with B_z alone. Figure 9 shows the time history of α_B, α_v, and $(\langle B^2 \rangle - B_0^2)/(8\pi P_0)$ for a typical B_z model (model V) with $A/\Omega = 3/4$, $B_x = B_y = 0$, $B_z \neq 0$ and $\beta = 1000$. The size of the simulation box and the number of grid points are the same as model T. The obtained α values for B_z models are generally greater than B_y models and now between 0.1 and 1. A tendency similar to this has been noted in computation by Hawley *et al.* (1994). As they already report, we need not put too many figures in the present paper.

Through three-dimensional MHD simulation, we have demonstrated that unstable eigenmodes appear in magnetized differentially rotating disks and that turbulent and chaotic magnetic field structures are created by the instability. Here we compare our theory with the results of three-dimensional MHD simulations by Hawley *et al.* (1994). Using the shearing box model, they simulated both the initially uniform vertical field models and uniform toroidal field models.

In vertical field models, the radial wavelength of growing modes increases with time and nearly axisymmetric two channel flow with large radial extent appears. This behavior is what we expect from our linear analysis. As we noticed in Sec. 2.3, when the vertical field is dominant, the width of the unstable eigenfunction depends on q as $\Delta x = (v_A/A)q^{-1/2}$. Since the growth rate increases by decreasing q, modes with longer wavelength both in x- and y-direction become dominant. When the instability-induced toroidal field becomes dominant,

however, the radial extent of the unstable mode shrinks to $\Delta x \sim v_A/A$. Thus the two channel flow breaks up and forms structures with size $\sim \beta^{-1/2}H$. When the plasma β is already decreased to $\beta \sim 10$ by the instability when this breakup occurs, the preferential radial size of growing modes will be $\sim 0.5H$. These theoretical expectations are consistent with the numerical results by Hawley *et al.* (1994).

In toroidal field models, since the radial width of the unstable eigenfunctions is independent of q, the radial size of growing modes is fixed to $\Delta x \sim v_A/A$, while more rapidly growing modes with smaller q are excited and become dominant. When $\beta = 100$, the radial size is $\Delta x \sim 0.2H$. This size is consistent with that of growing cells in model Y1 ($\beta = 100$) reported by Hawley *et al.* (1994). In a later stage, the radial sizes of unstable eigenmodes increase because v_A increases. Although the shapes of growing modes are highly elongated in y-direction, the system does not approach the axisymmetric state even in the later stage. This behavior is theoretically expected because the most rapidly growing mode satisfies $k_\parallel H \sim \Omega H/v_A = C_s/v_A$. Even if the vertical magnetic fields are generated by the instability, k_z alone cannot satisfy this criterion when v_A approaches C_s. Thus the growing mode inevitably has nonzero k_y.

The numerical results by Hawley *et al.* (1994) show saturation of the growth of magnetic fluctuations but they offered no physical mechanism of saturation. As we have shown in Sec. 3, the enhanced resistivity by tangled magnetic fields can provide such a mechanism that is consistent with the various observed characteristics.

5 SUMMARY AND DISCUSSION

We have shown that in the presence of nonzero electric resistivity, there is a threshold magnetic field strength below which the magnetic shearing instability is stabilized. By using the magnetic fluctuation dependent resistivity and applying the marginal stability theory in a self-consistent fashion, we have found that the magnetic viscosity parameter of a fully ionized

accretion disk is $\alpha_B \sim 0.001 - 1$, depending on magnetic configurations and to an extent on models of anomalous resistivity. It remains, however, to be important to investigate the detailed behavior of anomalous resistivity.

One of important implications of the present theory is that α_B depends on the temperature of accretion disks. Our theory indicates that in the innermost region of accretion disks around stellar mass black holes or neutron stars where $T \sim 10^7 K$, the magnetic viscosity parameter is $\alpha_B = \mathrm{O}(0.1)$ where the disk is fully ionized. In lower temperature ($T < 10^4 K$) disks whose ionization level is low, we expect that the saturation level of magnetic fluctuations is lower because the electron density is proportional to χ_e. Since α_B determined from Eq. (32) is proportional to χ_e, the magnetic viscosity drastically decreases when the hydrogen recombination occurs.

The quasiperiodic activity in dwarf novae is theoretically attributed to the thermal limit cycle behavior in accretion disks which appears when the hydrogen recombination accompanies in the disk (e.g., Meyer & Meyer-Hofmeister 1981; Cannizzo, Ghosh, & Wheeler 1982; Mineshige & Osaki 1983). In such theories, it is *assumed* that $\alpha \sim 0.1$ in the bursting phase and $\alpha \sim 0.02$ in the quiescent phase in order to fit the theoretical duration of the quiescent and bursting phases with the observation. According to our theory, the smaller α in the quiescent phase may be explained by the switch off of the magnetic viscosity due to the hydrogen recombination and thus a lower α_B (Eq. (32)).

Next, let us discuss in star forming regions whether large resistivity can stabilize the magnetic shearing instability. Since the temperature of protostellar disks is so low ($T \sim 100 K$) that even the original collisional resistivity is substantial. We assume that the thickness of the protostellar disk is $H \sim 10^{14}$ cm and the number density is $n \sim 10^{10}\mathrm{cm}^{-3}$. Using the resistivity expression in a partially ionized medium (e.g., Norman & Heyvaerts 1985), we obtain $\eta \sim 3 \times 10^{-5} H C_s$. By applying Eq. (27), we find the critical field strength for poloidal magnetic shearing instability is $B_{zc} \sim 10^{-6} G$, which is much smaller than the

strength of large-scale poloidal magnetic field in protostellar disks. Thus, the magnetic shearing instability can grow even in protostellar disks. The saturation level of the instability, however, will be low due to the low ionization level. The observational constraint on the value of α in protostellar disks comes from the excess infrared spectra around T Tauri stars (Adams, Lada, & Shu 1987), which suggests the presence of a viscous disk. The infrared excess vanishes on timescales of several 10^6 yr (Strom, Edwards, & Strom 1989). Since the viscous evolution time scale when $T = 100K$, $R = 10^{15}$cm, and $H/R = 0.1$ is $t_v \sim (\alpha C_s)^{-1}(R^2/H) \sim (3/\alpha) \times 10^3$ yr, the viscosity parameter α is the order of 10^{-3}. Such a smaller value of α is consistent with the above discussion that the magnetic viscosity is turned off in protostellar disks.

The amplification of a seed magnetic field by the magnetic shearing instability also occurs in spiral galaxies. In the region where the rotation speed decreases with radius ($A/\Omega > 0.5$), the magnetic field can be amplified up to $1/\beta > 0.01$ by this mechanism. The resulting predominantly toroidal magnetic field ($q = k_y^2/k_z^2 \sim 0.01$) is consistent with observations of magnetic fields in spiral galaxies (e.g., Sofue *et al.* 1986; Tajima & Gilden 1987). The strength of magnetic fields ($\beta \sim 1$) in spiral galaxies, however, suggests that other amplification mechanisms such as the resonance with the spiral arm (Chiba & Tosa 1990) are important, or the saturation level of the instability is higher.

When the magnetic shearing instability grows in spiral galaxies, the interstellar gas will fall toward the center by magnetic viscosity. The time scale of infall is roughly $t_v \sim 10^9(1/\alpha)(R/10\mathrm{kpc})(C_s/10\mathrm{kms}^{-1})^{-1}(H/R)^{-1}$ yr. This time scale is longer than the age of universe in the outer part where the rotation curve is flat ($A/\Omega \sim 0.5$). In the middle part ($R = 1-3\,\mathrm{kpc}$ in our galaxy) where $A/\Omega > 0.5$, it is possible that viscous infall occurs within 10^{10} yr. The accretion rate $\dot{M} \sim 10^2\alpha(R/10\,\mathrm{kpc})(C_s/10\mathrm{kms}^{-1})(n/1\mathrm{cm}^{-3})(H/R)^2 M_\odot/\mathrm{yr}$ can exceed $0.1M_\odot/\mathrm{yr}$, required to explain the activity of Seyfert galaxies.

In this paper, we have neglected the effect of gravity in vertical direction. When the

vertical gravity is included, strongly generated toroidal magnetic fields will escape from the disk into the corona by the Parker instability (Parker 1966; Horiuchi *et al.* 1988; Matsumoto *et al.* 1988,1990). The time scale of magnetic flux escape is $2-3H/v_A$ (Horiuchi *et al.* 1988; Matsumoto *et al.* 1988). In Keplerian disks whose magnetic field strength is determined by the marginal stability ($\beta \sim 10$), this time scale is 2–3 times longer than the growth time of the magnetic shearing instability. When the saturation level of the magnetic fields strength is higher either by stronger differential rotation, or by smaller anomalous resistivity, the growth rate of the magnetic shearing instability will be comparable to that of the Parker instability. In such cases, the Parker instability becomes important to determine the saturation level of magnetic fluctuations and the magnetic viscosity. The effect of the Parker instability on the magnetic viscosity has been taken into account phenomenologically in the model of hydromagnetic turbulence in accretion disks (Kato & Horiuchi 1985, 1986; Horiuchi & Kato 1990; Kato & Yoshizawa 1993), and in the model equations of the evolution of magnetic fields in accretion disks (Tout & Pringle 1992). It is recalled that when the magnetic field is sufficiently strong ($\beta \ll 10$), even the Parker instability is stabilized (Shibata, Tajima & Matsumoto 1990). The observed value of α_B in the simulation of Kaisig, Tajima & Lovelace (1992), in which the destabilized modes are generically similar to the one under consideration, is not inconsistent with our theoretical value. More quantitative study using 3D MHD code is in progress, and will be reported in our future paper (Kaisig, Tajima & Matsumoto 1994).

The authors thank M. Kaisig, S. Kato, W. Kley, S. Mineshige, K. Shibata, and F. Waelbroeck for discussions. We also thank M. LeBrun and G. Furnish for supplying us the PLPLOT plotting package. This work is supported by NSF ATM-91-13576.

5.1 REFERENCES

1. Adams, F. C., Lada, C., and Shu F. H., Ap.J. **312**, 788 (1987).

2. Balbus, S. A., and Hawley, J. F., Ap.J. **376**, 214 (1991).

3. Balbus, S. A., and Hawley, J. F., Ap.J. **400**, 610 (1992).

4. Cannizzo, J. K., Ghosh, P., and Wheeler, J. C., Ap.J. **260**, L83 (1982).

5. Cannizzo, J. K., Shafer, A. W., and Wheeler, J. C., Ap.J. **333**, 227 (1988).

6. Chandrasekhar, S., *Hydrodynamic and Hydromagnetic Stability* (Oxford, Clarendon Press, 1961), p. 384.

7. Chiba, M., and Tosa, M., MNRAS **244**, 714 (1990).

8. Drury, L. O'C, MNRAS **217**, 821 (1985).

9. Eardley, D. M., and Lightman, A. P., Ap.J. **200**, 187 (1975).

10. Foglizzo, T., and Tagger, M., A&A **287**, 297 (1994).

11. Glaztel, W., MNRAS **225**, 227 (1987).

12. Goldreich, P., Goodman, J., and Narayan, R., MNRAS **221**, 339 (1986).

13. Goldreich, P., and Lynden-Bell, D., MNRAS **130**, 125 (1965).

14. Goodman, J., and Xu, G., Ap.J. **432**, 213 (1994).

15. Hanawa, T., A&A **185**, 160 (1987).

16. Hawley, J. F., and Balbus, S. A., Ap.J. **376**, 223 (1991).

17. Hawley, J. F., and Balbus, S. A., Ap.J. **400**, 595 (1992).

18. Hawley, J. F., Gammie, C. F., and Balbus, S. A. 1994, preprint.

19. Horiuchi, T., and Kato, S., PASJ **42**, 661 (1990).

20. Horiuchi, T., Matsumoto, R., Hanawa, T., and Shibata, K., PASJ **40**, 147 (1988).

21. Horton, W., Tajima, T., and Galvao, R., in *Magnetic Reconnection in Space and Laboratory Plasmas*, Ed. Hones, and Edward W. (American Geophysical Union, 1984), p. 45.

22. Ichimaru, S., Ap.J. **202**, 528 (1975).

23. Ichimaru, S., Ap.J. **208**, 701 (1977).

24. Kaisig, M., A&A **218**, 89 (1989).

25. Kaisig, M., Tajima, T., and Lovelace, R. V. E., Ap.J. **386**, 83 (1992).

26. Kaisig, M., Tajima, T., and Matsumoto, R. 1994, in preparation.

27. Kato, S., PASJ **36**, 55 (1984).

28. Kato, S., and Horiuchi, T., PASJ **37**, 399 (1985).

29. Kato, S., and Horiuchi, T., PASJ **38**, 313 (1986).

30. Kato, S., PASJ **9**, 645 (1987).

31. Kato, S., and Yoshizawa, A., PASJ **45**, 103 (1993).

32. Kley, W., Papaloizou, J. C. B., and Lin, D. N. C., Ap.J. **416**, 679 (1993).

33. Knobloch E., MNRAS **255**, 259 (1992).

34. Kumar, S., Coleman, C. S., and Kley, W., MNRAS **266**, 379 (1994).

35. Lin, D. N. C., and Papaloizou, J. C. B., MNRAS **191**, 37 (1980).

36. Manheimer, W., and Boris, J. P., Comments Plasma Phys. Contr. Fusion **3**, 15 (1977).

37. Matsumoto, R., Horiuchi, T., Shibata, K., and Hanawa, T., PASJ **40**, 171 (1988).

38. Matsumoto, R., Horiuchi, T., Hanawa, T., and Shibata, K., Ap.J. **356**, 259 (1990).

39. Matsumoto, R., and Shibata, K. 1992, PASJ **44**, 167 (1992).

40. Matsumoto, R., Tajima, T., Shibata, K., and Kaisig, M., Ap.J. **414**, 357 (1993).

41. Matsumoto, R., Tajima, T., and Shibata, K. 1994, in preparation.

42. Meyer, F., and Meyer-Hofmeister, E., A&A **104**, L10 (1981).

43. Miller, R. L., Waelbroeck, F. L., Hassam, A. B., and Waltz, R. E. 1994, preprint.

44. Mineshige, S., and Osaki, Y., PASJ **35**, 377 (1983).

45. Mouschovias, T. Ch, and Paleologou, E. V., Ap.J. **246**, 48 (1981).

46. Norman, C., and Heyvaerts, J., A&A **147**, 247 (1985).

47. Papaloizou, J. C. B., and Pringle, J. E., MNRAS **208**, 721 (1984).

48. Parker, E. N., Ap.J. **145**, 811 (1966).

49. Pudritz, R. E, MNRAS **195**, 881 (1981).

50. Richtmyer, R. O., and Morton, K. W., *Differential Methods for Initial Value Problems (2nd ed.)* (New York: Interscience, 1967)), chap. 13 .

51. Rubin, E., and Burstein, S. Z., J. Comput. Phys. **2**, 17 (1967).

52. Ross, D. W., Chen, G. L., and Mahajan, S. M., Phys. Fluids **25**, 652 (1982).

53. Shakura, N. I., and Sunyaev, R. A., A&A **24**, 337 (1973).

54. Shibata, K., Tajima, T., and Matsumoto, R., Ap.J. **350**, 295 (1990).

55. Shibata, K., and Uchida, Y., PASJ **38**, 631 (1986).

56. Sofue, Y., Fujimoto, M., and Wielebinski, R., ARA&A **24**, 459 (1986).

57. Stone, J. M., and Norman, M. L. 1994, preprint.

58. Strom, S., Edwards, S., and Strom, K. M. 1989, Formation and Evolution of Planetary Systems, eds. H.A. Weaver and L. Danly (Cambridge University Press), p. 91

59. Tajima, T., and Gilden, D., Ap.J. **320**, 741 (1987).

60. Tajima, T., Horton, W., Morrison, P. J., Schutkeker, J., Kamimura, T., and Mima, K., Phys. Fluids B **3**, 938 (1991).

61. Tajima, T., Kishimoto, Y., LeBrun, M. J., Gray, M. G., Kim, J-Y., Horton, W., Wong, V., and Kotchenreuther, M. 1994, in *AIP conference proceedings 284, US-JAPAN Workshop on Ion Temperature Gradient-Driven Turbulent Transport*, Eds. W. Horton, M. Wakatani, A. Wootton, p. 255 .

62. Tout, C. A., and Pringle, J. E., MNRAS **259**, 604 (1992).

63. Uchida, Y., Matsumoto, R., Hirose, S., and Shibata, K., in *Primordial Nucleosynthesis and Evolution of Early Universe*, eds. K. Sato, and J. Audouze (Kluwer Academic Publishers, 1991), p. 409.

64. Uchida, Y., and Shibata, K., PASJ **37**, 515 (1985).

65. Velinhov, E. P., Soviet JETP **35**, 995 (1959).

66. Vishniac, E. T., and Diamond, P., Ap.J. **398**, 561 (1992).

67. Waelbroeck, F. L., Antonse, T. M., Guzdar, P. N., and Hassam, A. B., Phys. Fluids B 4, 2441 (1992).

68. Waelbroeck, F. L., Dong, J. Q., Horton, W., and Yushmanov, P. N. 1994, preprint.

69. Wisdom, J., and Tremaine, S., AJ, **95**, 925 (1988).

Table 1

Magnetic viscosity determined by marginal stability theory with Model 1

(a) with B_z start

A/Ω	$f(q=0)$	$\delta B^2/(4\pi\rho C_s^2)$	ω_A/Ω	α_B	α_v	Comment
0.85	5.7	3.6	0.99	1.8	1.33	
0.75	3.0	1.9	0.97	0.95	0.57	Kepler disk
0.50	1.0	0.64	0.87	0.50	0.17	Constant rotation speed
0.25	0.33	0.21	0.66	0.10	0.015	

(b) with B_y start

A/Ω	$q_{\max}$	$q_{\max}f(q_{\max})$	$\delta B^2/(4\pi\rho C_s^2)$	ω_A/Ω	α_B	α_v
0.85	0.015	0.009	0.011	0.6	0.0030	0.0017
0.75	0.01	0.005	0.0065	0.5	0.0018	0.0008
0.50	0.01	0.002	0.0025	0.5	0.0008	0.0002
0.25	0.0075	0.0007	0.0009	0.5	0.0004	0.00004

FIGURE CAPTIONS

Fig. 1. Examples of the eigenfunctions of the nonaxisymmetric magnetic shearing instability in a disk with the Keplerian velocity shear ($A/\Omega = 3/4$). Solid curve shows the real part and the dashed curve shows the imaginary part of the eigenfunction. The model parameters are $\omega_A = k_\parallel v_A = 0.1\Omega$ and $q = k_y^2/k_z^2 = 0.01$. (a) Fundamental mode (eigenvalue is $\omega = 0.0692\Omega i$). (b) Next nodal mode (eigenvalue is $\omega = 0.0357\Omega i$). The eigenfunctions are localized between $\xi = 2Ak_y x/\omega_A = \pm 1$.

Fig. 2. The $\omega_A = k_\parallel v_A$ and $q = k_y^2/k_z^2$ dependences of eigenvalues of the nonaxisymmetric magnetic shearing instability in the Keplerian disk. Solid curves and dashed curves show the growth rate $\gamma = \mathrm{Im}(\omega)$ and $\mathrm{Re}(\omega)$, respectively.

Fig. 3. Resistive stabilization of the magnetic shearing instability. Numerical solutions of the local dispersion relation for $\eta = 0$ (thin curves) and $\eta = 10^{-4} C_s H$ (thick curves) are displayed. The radial wavenumber k_x is assumed to be $k_x = 2\pi A/v_A$. The abscissa is the Alfvén frequency $\omega_A = k_\parallel v_A$.

Fig. 4. Result of the three-dimensional MHD simulation of the disk with the Keplerian velocity shear (model T). The unperturbed magnetic field is uniform and purely toroidal. The initial plasma β is 100. The isocontours of the azimuthal velocity perturbation δv_y in $z = 0.25H$ plane are shown. The contour step width is 0.5 in logarithmic scale. Solid curves and dashed curves represent the positive velocity, and the negative velocity, respectively.

Fig. 5. The same as figure 4 but for δv_y in the x-z-plane ($y = H$).

Fig. 6. The time variation of B_x along the line $y = H$ and $z = 0.25H$ for model T. The modes with wavelength $\Delta x \sim 0.2H$ preferentially grow. Exponential growth of an eigenmode is seen around $x = -0.1H$ during $t = 11.2/\omega - 16.4/\omega$.

Fig. 7. Magnetic field lines for model T in the eigenmode growth stage ($t = 8.4/\omega - 16.4/\omega$) and the nearly saturation stage ($t = 20.9/\omega - 25.0/\omega$).

Fig. 8. The time history of (a) $\alpha_B = -\langle B_x B_y \rangle / (4\pi P_0)$, (b) $\rho_0 \langle v_x v_y \rangle / P_0$, and (c) the magnetic fluctuation $(\langle B^2 \rangle - B_0^2)/(8\pi P_0)$ for toroidal field model (model T).

Fig. 9. The time history of (a) $\alpha_B = -\langle B_x B_y \rangle / (4\pi P_0)$, (b) $\rho_0 \langle v_x v_y \rangle / P_0$, and (c) the magnetic fluctuation $(\langle B^2 \rangle - B_0^2)/(8\pi P_0)$ for vertical field model (model V).

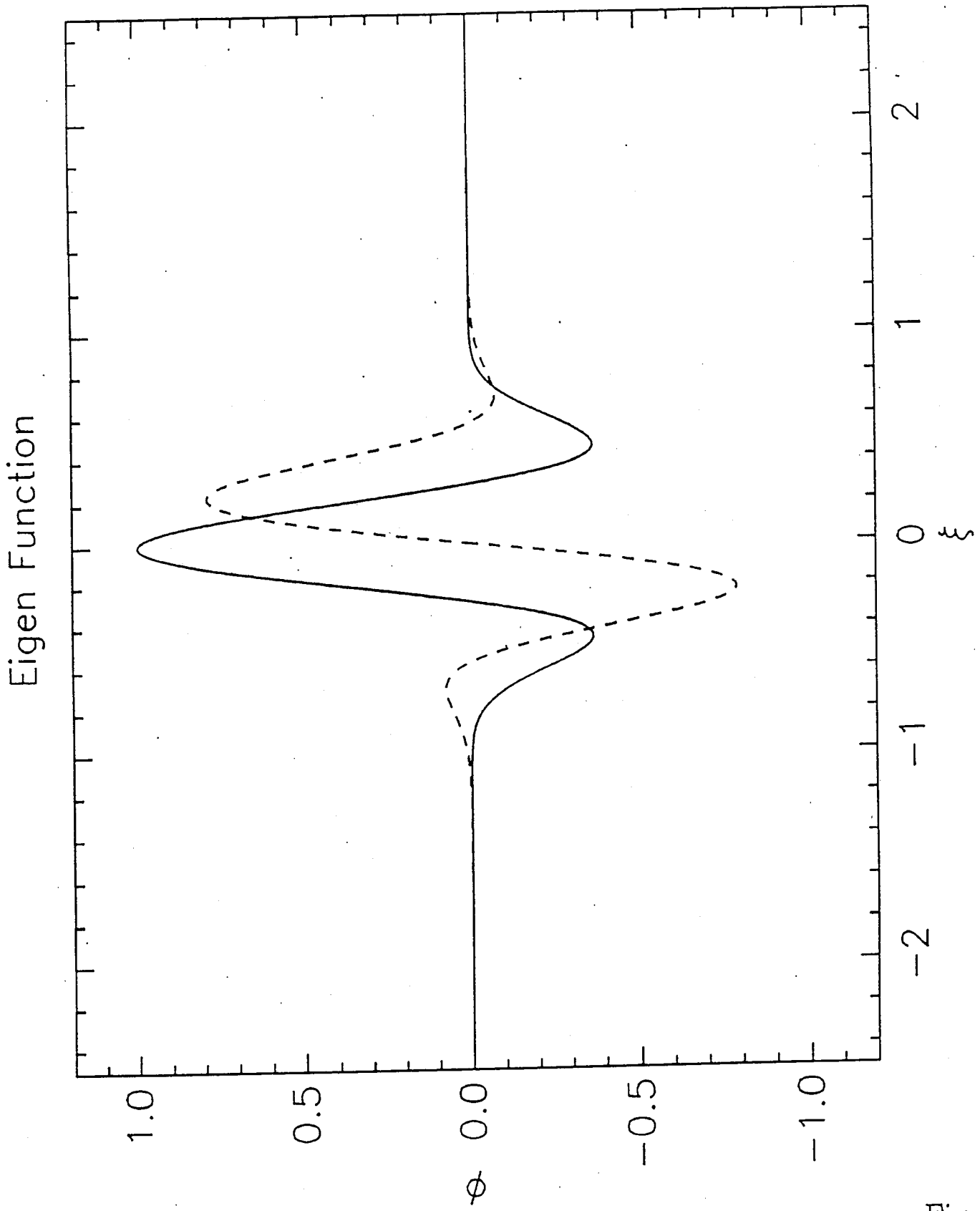

Fig. 1a

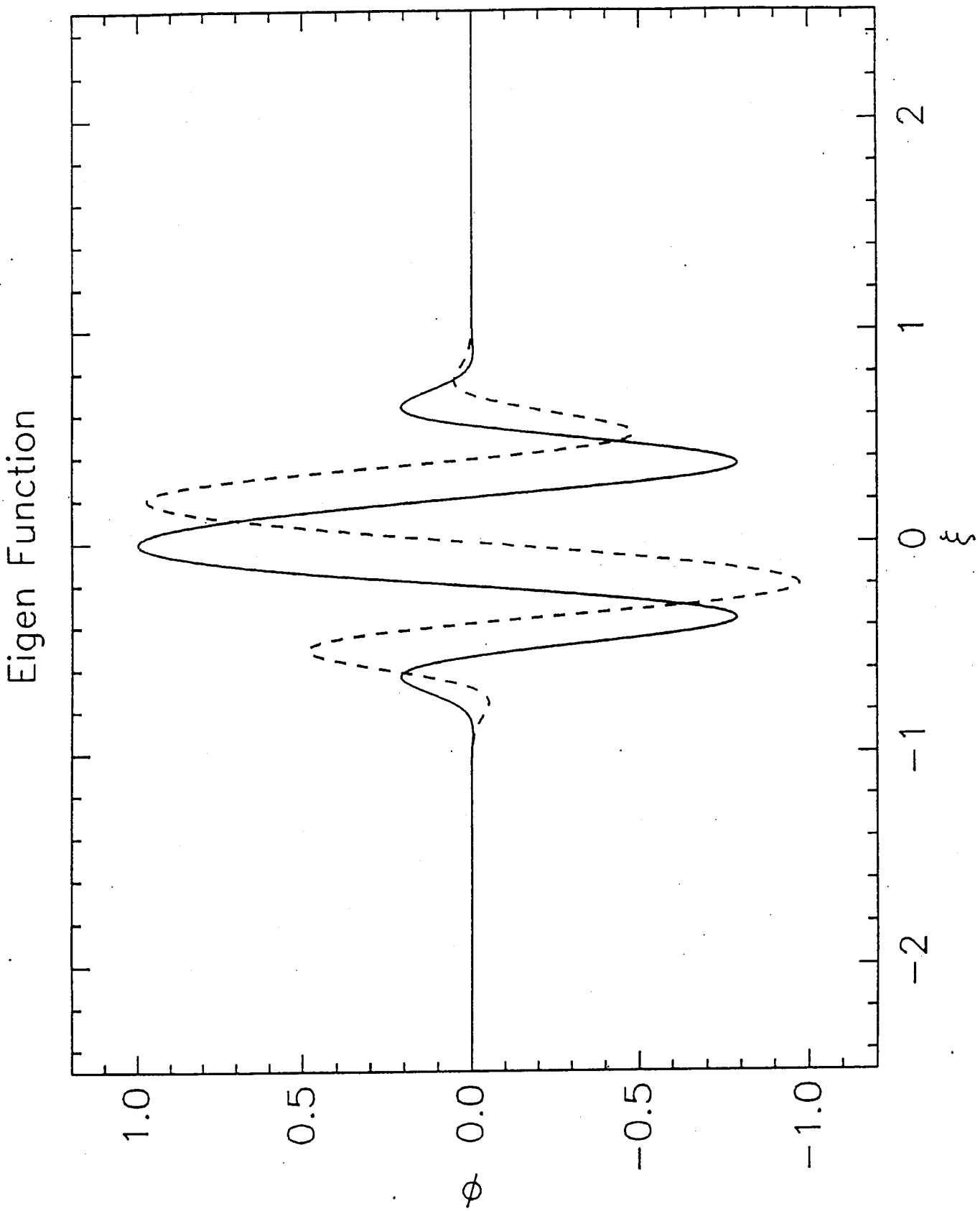

Fig. 1b

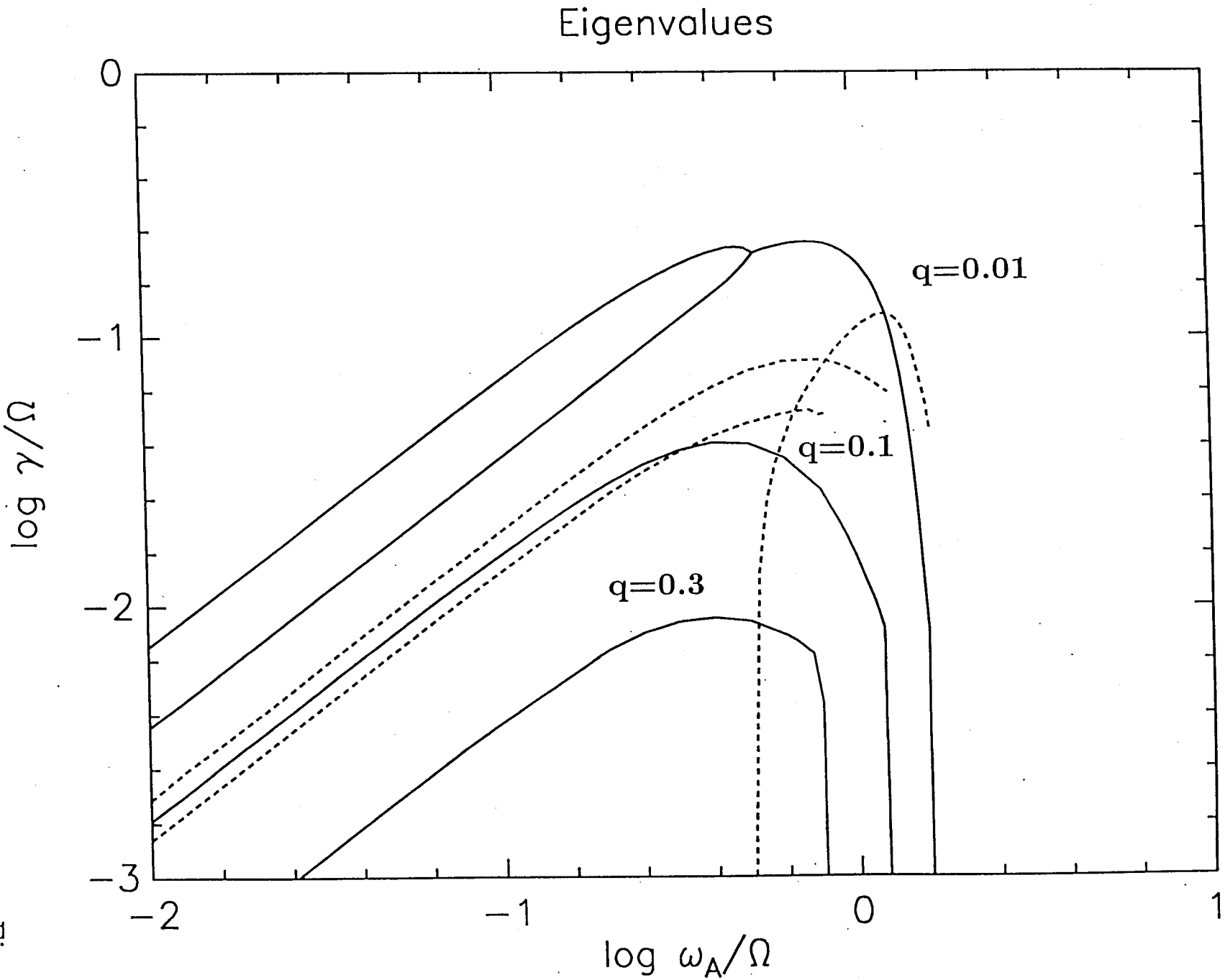

Fig. 2

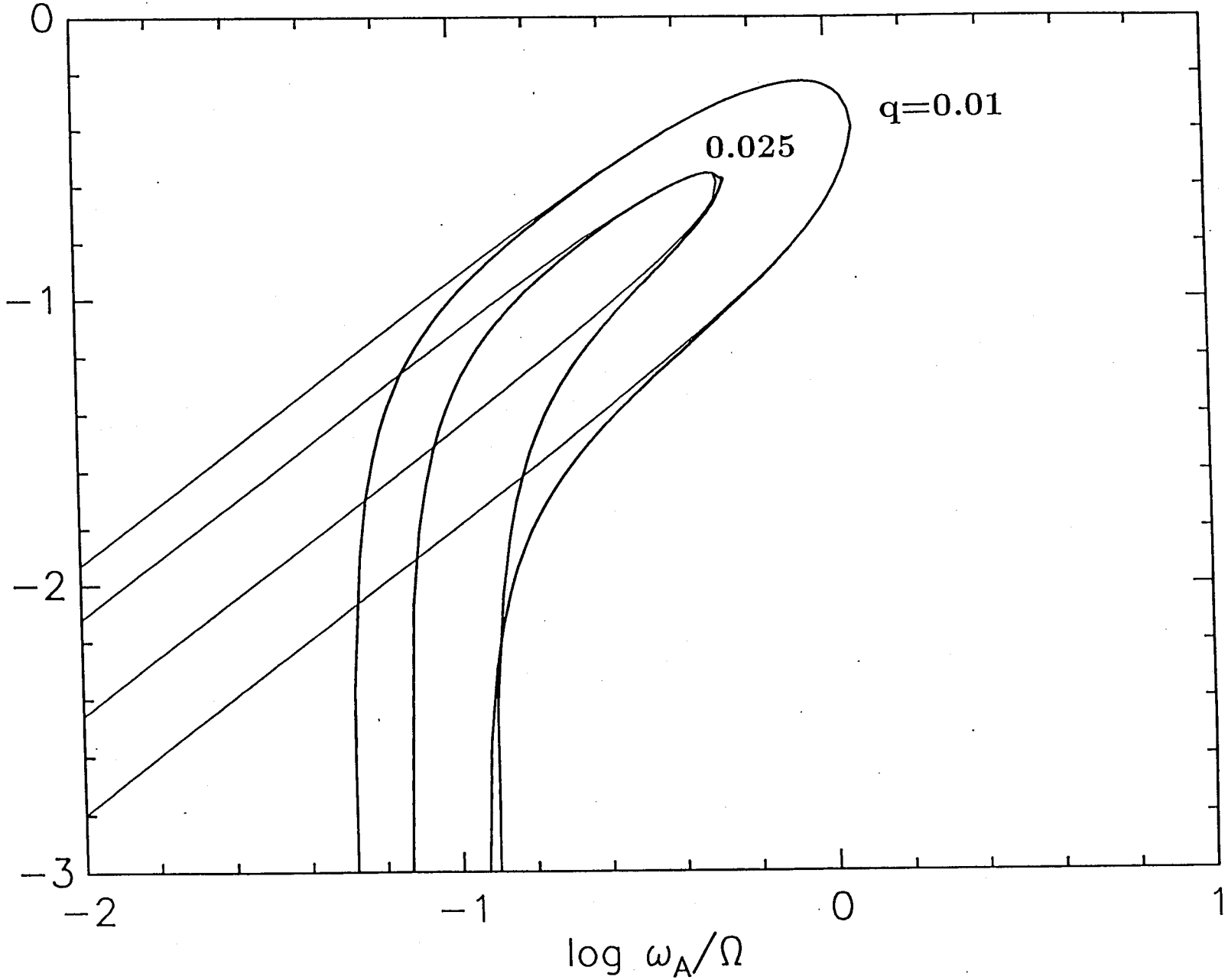

Fig. 3

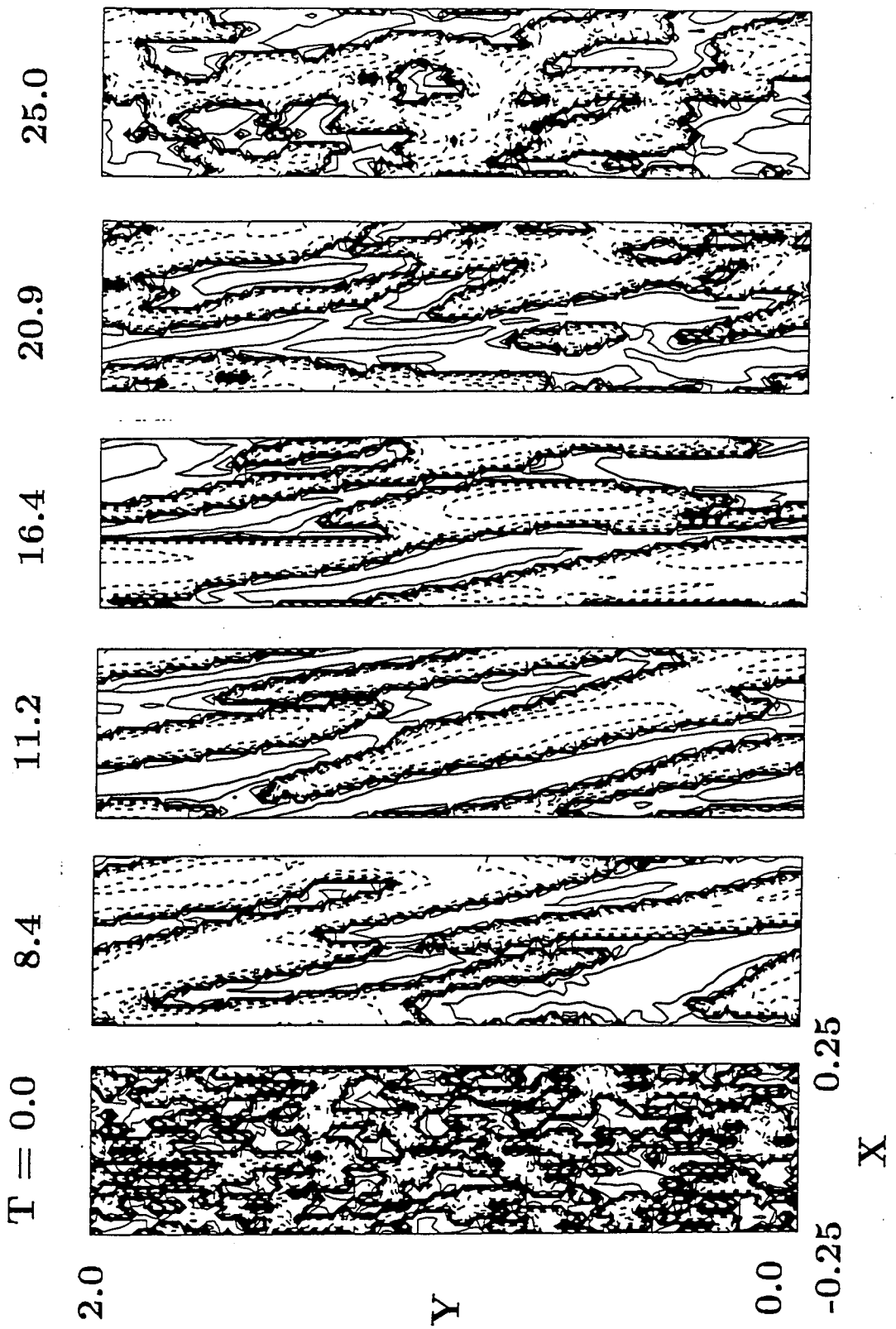

Fig. 4

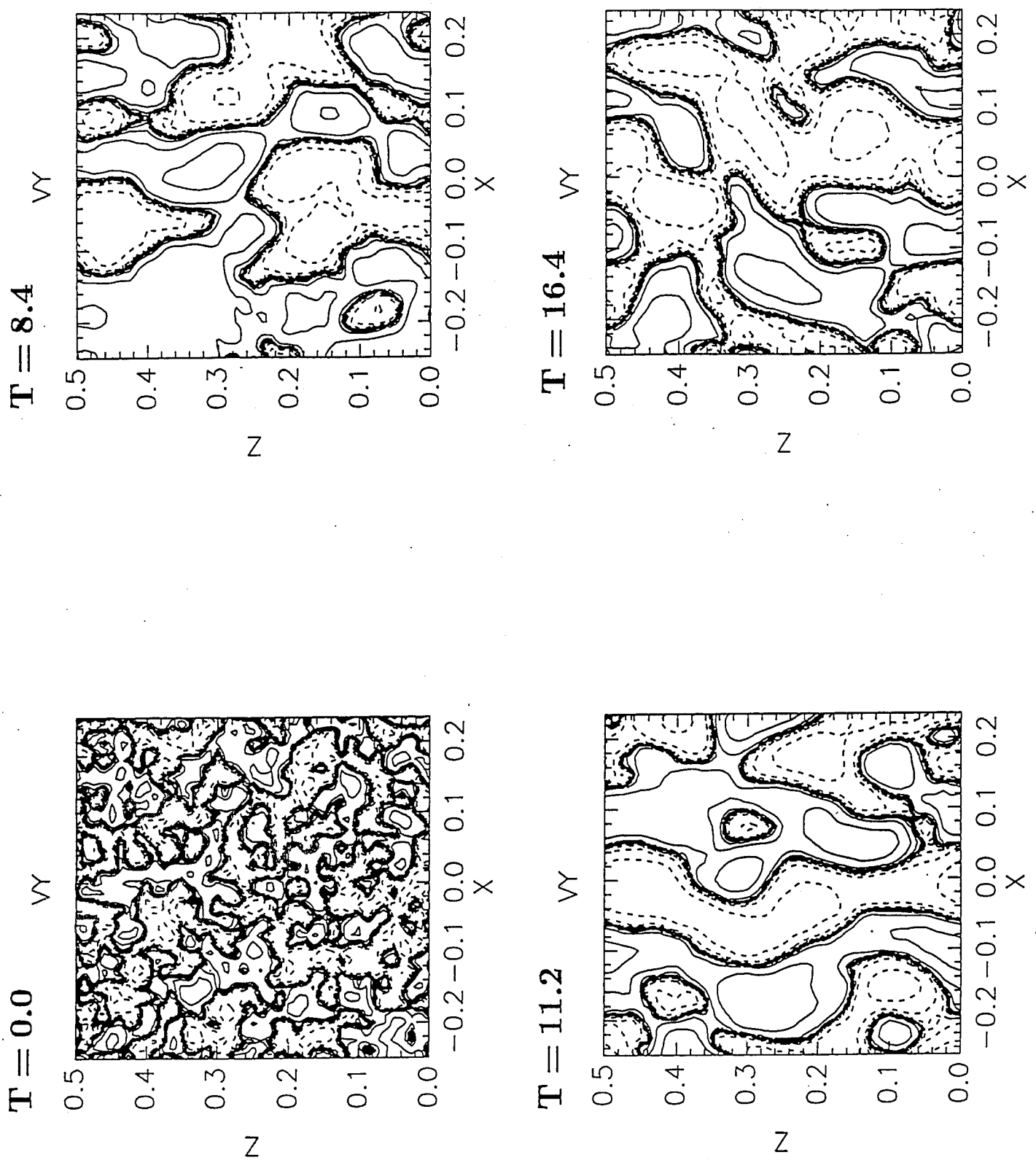

Fig. 5

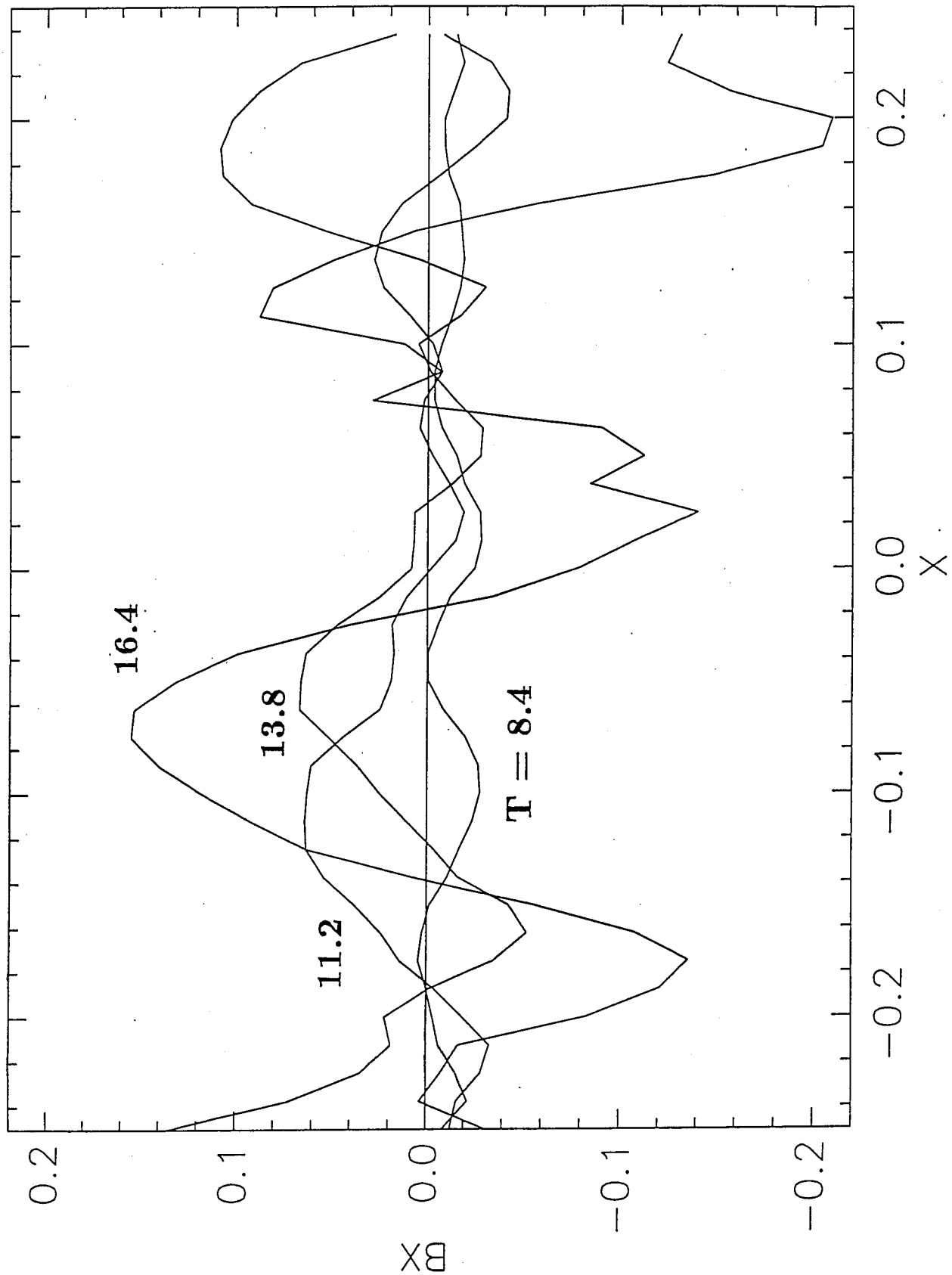

Fig. 6

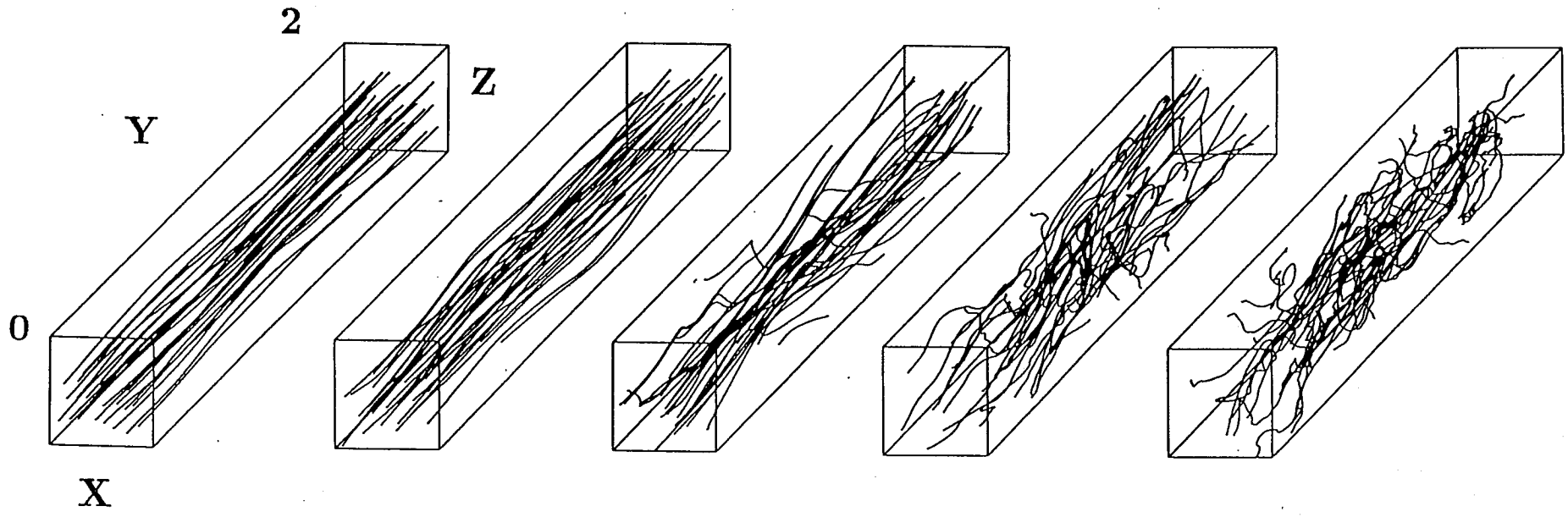

T = 8.4 11.2 16.4 20.9 25.0

Fig. 7

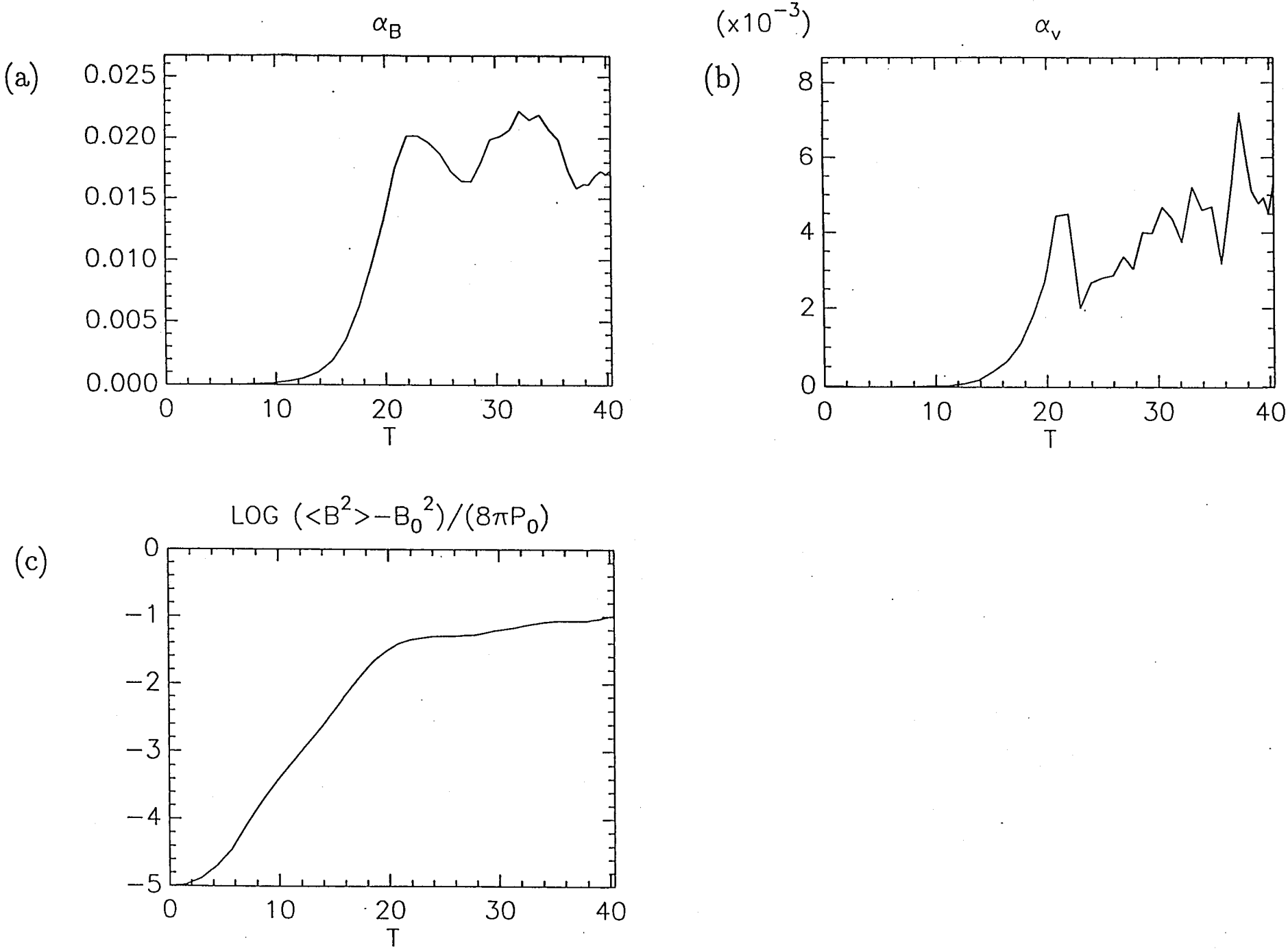
(a)
α_B
0.025
0.020
0.015
0.010
0.005
0.000
0
10
20
30
40
T
(b)
$(x10^{-3})$
α_v
8
6
4
2
0
0
10
20
30
40
T
(c)
LOG $(<B^2>-B_0^2)/(8\pi P_0)$
0
−1
−2
−3
−4
−5
0
10
20
30
40
T

Fig. 8

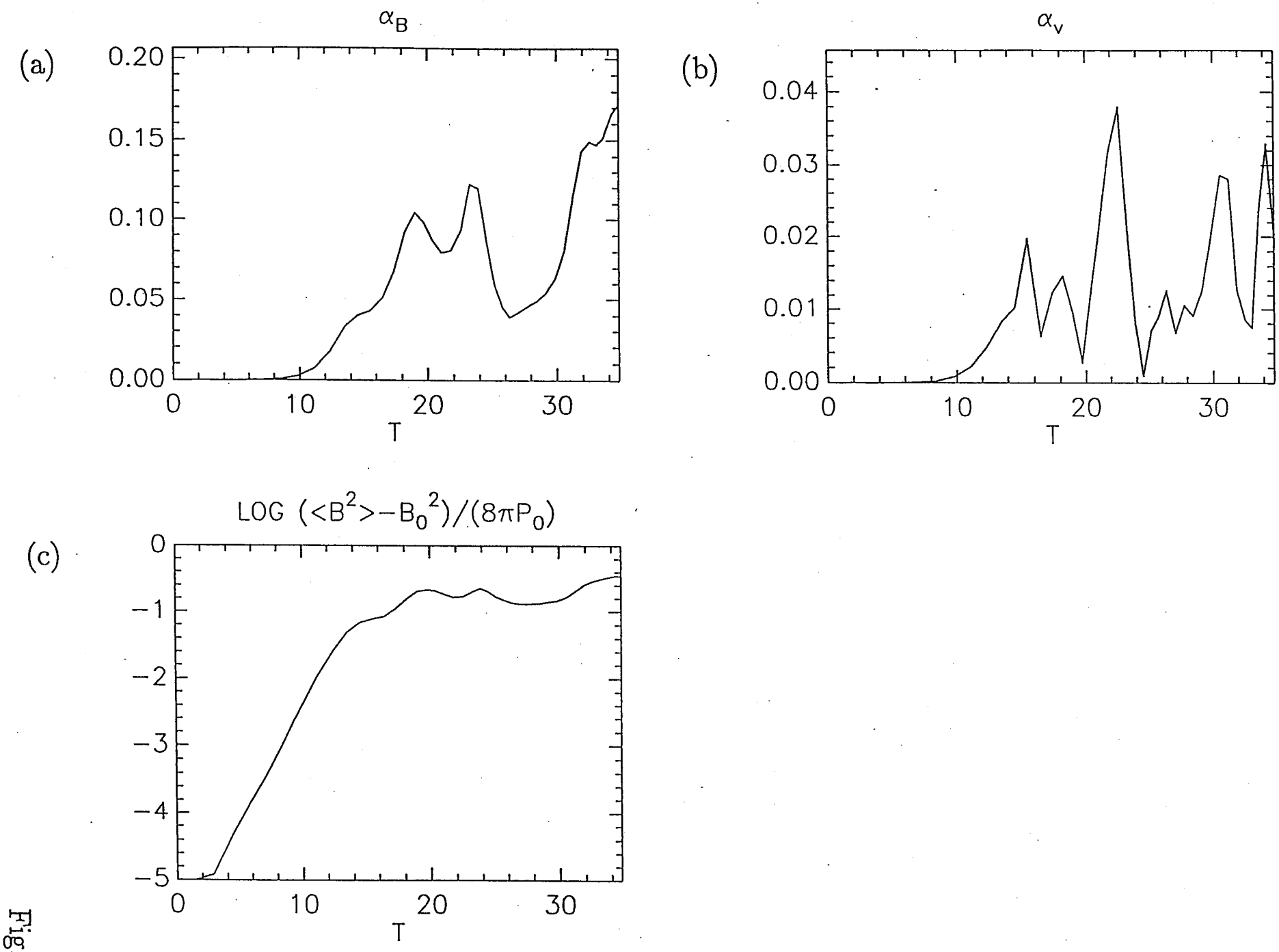
(a)
α_B
0.20
0.15
0.10
0.05
0.00
0
10
20
30
T
(b)
α_v
0.04
0.03
0.02
0.01
0.00
0
10
20
30
T
(c)
LOG $(<B^2>-B_0^2)/(8\pi P_0)$
0
−1
−2
−3
−4
−5
0
10
20
30
T

Fig. 9